Reduced sialylation triggers homeostatic synapse and neuronal loss in middle-aged mice

Christine Klaus, Jan N. Hansen, Aurélien Ginolhac, Deborah Gérard, Vinayaga S. Gnanapragassam, Rüdiger Horstkorte, Charlotte Rossdam, Falk F. R. Büttner, Thomas Sauter, Lasse Sinkkonen, Harald Neumann, Bettina Linnartz-Gerlach

Angaben zur Veröffentlichung / Publication details:

Klaus, Christine, Jan N. Hansen, Aurélien Ginolhac, Deborah Gérard, Vinayaga S. Gnanapragassam, Rüdiger Horstkorte, Charlotte Rossdam, et al. 2020. "Reduced sialylation triggers homeostatic synapse and neuronal loss in middle-aged mice." *Neurobiology of Aging* 88: 91–107. https://doi.org/10.1016/j.neurobiolaging.2020.01.008.

Neurobiology of Aging 88 (2020) 91–107

Contents lists available at ScienceDirect

Neurobiology of Aging

journal homepage: www.elsevier.com/locate/neuaging

Reduced sialylation triggers homeostatic synapse and neuronal loss in middle-aged mice

Christine Klaus [a], Jan N. Hansen [b], Aurélien Ginolhac [c], Deborah Gérard [c], Vinayaga S. Gnanapragassam [d], Rüdiger Horstkorte [d], Charlotte Rossdam [e], Falk F.R. Buettner [e], Thomas Sauter [c], Lasse Sinkkonen [c], Harald Neumann [a,*], Bettina Linnartz-Gerlach [a]

[a] Neural Regeneration, Institute of Reconstructive Neurobiology, Medical Faculty and University Hospital of Bonn, University of Bonn, Bonn, Germany
[b] Biophysical Imaging, Institute of Innate Immunity, Medical Faculty, University of Bonn, Bonn, Germany
[c] Epigenetics Team, Systems Biology Group, Life Sciences Research Unit, University of Luxembourg, Belvaux, Luxembourg
[d] Institute for Physiological Chemistry, Medical Faculty, Martin Luther University Halle-Wittenberg, Halle (Saale), Germany
[e] Institute of Clinical Biochemistry, Hannover Medical School, Hannover, Germany

ARTICLE INFO

Article history:
Received 9 September 2019
Received in revised form 6 January 2020
Accepted 14 January 2020
Available online 21 January 2020

Keywords:
Microglia
Neuroinflammation
Sialic acid
Aging
Neurodegeneration
Glycocalyx
GNE

ABSTRACT

Sialic acid-binding Ig-like lectin (Siglec) receptors are linked to neurodegenerative processes, but the role of sialic acids in physiological aging is still not fully understood. We investigated the impact of reduced sialylation in the brain of mice heterozygous for the enzyme glucosamine-2-epimerase/N-acetylmannosamine kinase (GNE+/−) that is essential for sialic acid biosynthesis. We demonstrate that GNE+/− mice have hyposialylation in different brain regions, less synapses in the hippocampus and reduced microglial arborization already at 6 months followed by increased loss of neurons at 12 months. A transcriptomic analysis revealed no pro-inflammatory changes indicating an innate homeostatic immune process leading to the removal of synapses and neurons in GNE+/− mice during aging. Cross-breeding with complement C3-deficient mice rescued the earlier onset of neuronal and synaptic loss as well as the changes in microglial arborization. Thus, sialic acids of the glycocalyx contribute to brain homeostasis and act as a recognition system for the innate immune system in the brain.

1. Introduction

All neurons are covered by a rich glycan-coated surface, the neuronal glycocalyx. The terminal ends of the neuronal glycocalyx are masked by sialic acids, anionic sugars that are considered to play a crucial role in cell-cell recognition during physiological and pathological processes (Cohen and Varki, 2010; Linnartz-Gerlach et al., 2014; Schauer, 2009). Sialic acids could act as biological recognition sites for the innate immune system in several organs (Blaum et al., 2015; Crocker et al., 2007). They have been described as “self” ligands or “don't eat me” signals (Varki, 2011) and might function as an indicator for cellular well-being (Rachmilewitz, 2010). Microglia, the innate immune cells of the brain, constantly survey the brain parenchyma and monitor the neuronal well-being with a wide array of receptors including the sialic acid-binding immunoglobulin-like lectins (Siglecs).

The sialylation pattern continuously changes during physiological and pathological conditions (Wei and Wang, 2019). Desialylation was well studied in erythrocytes and there, might be the first step of cellular “glycoprotein/-lipid aging”, as demonstrated for its association with cellular senescence and its correlation with oxidative stress markers (Lutz and Bogdanova, 2013; Mehdi et al., 2012). The desialylation of erythrocytes also provokes cell surface phosphatidylserine exposure (Qadri et al., 2018). Interestingly, re-sialylation of senescent erythrocytes increases their circulation lifespan (Huang et al., 2016). Furthermore, polysialylation plays a crucial role in early brain development with reaching peak expression perinatally (Schnaar et al., 2014). Recently, the sialic acid activating enzyme CMP-sialic acid synthase (CMAS) was also identified as key regulator of inhibiting microglial phagocytosis confirming the functional role of sialic acids in the brain (Pluvinage et al., 2019).

* Corresponding author at: Neural Regeneration, Institute of Reconstructive Neurobiology, Medical Faculty and University Hospital of Bonn, University of Bonn, Bonn, Germany. Tel.: +492286885541; fax: +492286885501.
E-mail address: harald.neumann@uni-bonn.de (H. Neumann).

0197-4580/
https://doi.org/10.1016/j.neurobiolaging.2020.01.008

To mimic a glycocalyx with reduced sialylation, we analyzed mice heterozygous for the bifunctional enzyme glucosamine-2-epimerase/N-acetylmannosamine kinase (GNE; Schwarzkopf et al., 2002), the rate-limiting enzyme of the sialic acid biosynthesis (Keppler, 1999). GNE+/− mice showed an overall reduction of membrane-bound sialic acids in all organs by approximately 25% compared to wildtype littermate controls (Gagiannis et al., 2007; Schwarzkopf et al., 2002).

Already at 6 months of age, we observed reduced synapse numbers in the hippocampus of GNE+/− mice. At later time points, we observed that the altered sialylation led to accelerated neuronal loss in the hippocampus and substantial neuronal loss in the substantia nigra in GNE+/− mice. Interestingly, the neuronal loss was not accompanied by major pro-inflammatory changes in the brain. Only minor but visible changes were detected in the arborization of microglia. By crossbreeding the GNE+/− mice with mice deficient for complement component 3 (C3), we rescued the loss of synapses and neurons, as well as the microglial changes. Thus, data demonstrate an important role of sialic acids as protective carbohydrates against complement-mediated loss of synapses and neurons in the physiological aging mouse brain.

2. Results

2.1. GNE+/− mice are a suitable model for reduced brain sialylation

GNE+/− mice exhibit an overall reduction of membrane-bound sialic acids by ~ 25%, but without any obvious defects in organ architecture (Gagiannis et al., 2007). To validate GNE+/− mice as a suitable in vivo model of a desialylated glycocalyx in the brain, we first quantified the transcription levels of the bifunctional enzyme GNE in the brain at different time points (Suppl. Fig. 1). Transgenic GNE+/− mice showed an overall reduction of mRNA levels by 54% compared to wildtype (GNE+/+) littermates ($p < 0.001$). In detail, *Gne* transcript levels were reduced from an average of 0.7 ± 0.1 fold change (FC) in 1 month old wildtype mice to 0.3 ± 0.0 FC in age-matched GNE+/− mice, from 1.0 ± 0.1 FC to 0.4 ± 0.0 FC ($p < 0.001$) in 3 month old mice, from 1.1 ± 0.1 FC to 0.5 ± 0.0 FC ($p < 0.001$) in 6 month old mice, from 1.0 ± 0.1 FC to 0.4 ± 0.1 FC ($p < 0.001$) in 9 month old mice, and from 1.0 ± 0.1 FC to 0.5 ± 0.0 FC ($p < 0.001$) in 12 month old mice (Suppl. Fig. 1).

Since GNE is a rate-limiting enzyme in the sialic acid biosynthesis, we next tested whether reduced *Gne* transcript levels result in reduced sialylation in the GNE+/− mouse model. To this end, we first employed a flow cytometry approach for quantifying the cell surface sialic acid levels on cells of whole brain homogenates (Suppl. Fig. 2). Levels of polysialic acids and sialic acid oligomers were measured at different ages with antibodies directed against polysialic acid (PSA-NCAM, NeuAc-α2-8_n with n > 10) that is mainly attached to the neural cell adhesion molecule (NCAM) or directed against the trisialic acid oligomers (A2B5, NeuAc-α(2−8) NeuAc-α(2−8) NeuAc (Hanashima et al., 2013); that are part of a c-series ganglioside subunit (Saito et al., 2001), respectively (Fig. 1A). Interestingly, there were remarkable changes in cell surface expression on brain cells from 3 to 12 months of age. In wildtype mice, the level of polysialic acids increased until 6 months of age and subsequently decreased (6 months vs. 12 months, $p < 0.001$), while the expression of trisialic acid oligomers of gangliosides showed the opposite. Levels of trisialic acid of gangliosides slightly decreased until 6 months of age and then continually increased with age up to 12 months. Overall, the relative median fluorescence intensity for polysialic acids and trisialic acid oligomers was lower in GNE+/− mice compared to wildtype mice at all time points measured. In detail, the detected relative median fluorescence intensity of polysialic acids decreased in wildtype mice from a mean of 100 ± 18.1% at 3 months, over 128.3 ± 13.8% at 6 months, to 90.7 ± 10.4% at 9 months and to 58.7 ± 12.2% at 12 months (Fig. 1A, left). In comparison, intensity levels in GNE+/− mice varied from 65.9 ± 11.0% at 3 months, to 61.3 ± 18.3% at 6 months, to 43.6 ± 14.0% at 9 months and to 51.5 ± 10.4% at 12 months. For A2B5, the relative median fluorescence intensity increased from 100 ± 26.3% at 3 months and 81.9 ± 21.2% at 6 months to 120.7 ± 12.0% at 9 months and 132.6 ± 27.9% at 12 months in wildtype mice, while it was slowly decreasing from 74.7 ± 16.2% at 3 months, to 62.6 ± 20.0% at 6 months, to 50.0 ± 15.4% at 9 months and to 48.2 ± 11.7% at 12 months in GNE+/− mice.

We second analyzed brain sections of 9 month old mice with antibodies directed against polysialic acid (NeuAc-α2-8_n with n > 10; PSA-NCAM) and trisialic acid oligomers (A2B5; Fig. 1B). Immunohistochemical staining of the hippocampus revealed a 54% reduction in polysialylation ($p = 0.039$; Fig. 1B) from 100 ± 21.1% in wildtype to 46.1 ± 5.3% in GNE+/− mice for PSA-NCAM, while levels of trisialic acid oligomers decreased to a lesser extent from 100 ± 12.1% in wildtype mice to 72.2 ± 25.5% in GNE+/− mice (A2B5 epitope; $p = 0.113$). Thus, reduced levels of polysialic acid in the hippocampus as detected by immunostaining at 9 months were in line with reduced cell surface levels shown by flow cytometry for overall brain tissue.

Furthermore, we third used an HPLC approach to determine the total amount of protein-bound sialic acid (Neu5Ac) in different brain regions (striatum, midbrain, hippocampus, cortex, cerebellum; Fig. 1C) and in peripheral organs (spleen, liver, kidney; Suppl. Fig. 3A). Interestingly, we saw different sialylation patterns for the distinct brain regions and organs that was dependent on the GNE genotype. At 3 months, the total protein-bound sialic acid levels were lower in the hippocampus of GNE+/− compared to wildtype mice (GNE+/−: 81.3 ± 1.6% vs. GNE+/+: 100.0 ± 2.9%; $p = 0.0013$) but levels were slightly higher in the cerebellum (GNE+/−: 115.7 ± 4.4% vs. GNE+/+: 100.0 ± 2.9%; $p = 0.025$; Fig. 1C). The effects of the GNE genotype were more visible at 12 months of age with a reduction in the hippocampus (GNE+/−: 83.5 ± 3.4% vs. GNE+/+: 100.0 ± 5.1%; $p = 0.036$), in the cortex (GNE+/−: 79.0 ± 2.4% vs. GNE+/+: 100.0 ± 1.7%; $p = 0.0004$) as well as in the cerebellum (GNE+/−: 82.8 ± 3.1% vs. GNE+/+: 100.0 ± 5.6%; $p = 0.036$) of GNE+/− mice compared to wildtype mice. In the periphery, the relative levels of protein-bound sialic acids were only slightly, but significantly, reduced in liver and kidney at 12 months of age in GNE+/− compared to wildtype mice (Suppl. Fig. 3A).

Finally, we analyzed the glycosphingolipid glycosylation by multiplexed capillary gel electrophoresis coupled to laser-induced fluorescence detection (xCGE-LIF) (Rossdam et al., 2019) in order to quantitatively compare ganglioside levels in wildtype and GNE+/− mice at 9 months of age (Suppl. Fig. 3B). The 4 major brain gangliosides in the adult brain (GM1, GD1a, GD1b, and GT1b) comprise 97% of all gangliosides (Tettamanti et al., 1973) and carry ~75% of the total brain sialic acids (Norton and Poduslo, 1973; Schnaar et al., 2014; Yu et al., 1988). Based on the currently available migration time database, numerous but not all peaks in the electropherograms could be assigned to defined glycan structures. Our analysis clearly revealed that the gangliosides GM1a and GD1a are the most abundant structures comprising more than 40% of all gangliosides. However, ganglioside levels were similar between wildtype and GNE+/− mice (Suppl. Fig. 3B).

Taken together, our data demonstrate that heterozygous knock out of GNE in younger mice mainly affects cell surface expression of polysialic acid levels of NCAM, whereas trisialic acid oligomers of gangliosides, that compromise less than 3% of the brain gangliosides, was affected in middle-aged animals. As we did not observe differences in the levels of major gangliosides, that carry glycan headgroups with mono- or disialic acid residues, it is hypothesized that mostly polysialylation of NCAM and trisialylation as part of the c-series gangliosides are affected in GNE+/− mice compared to wildtype controls.

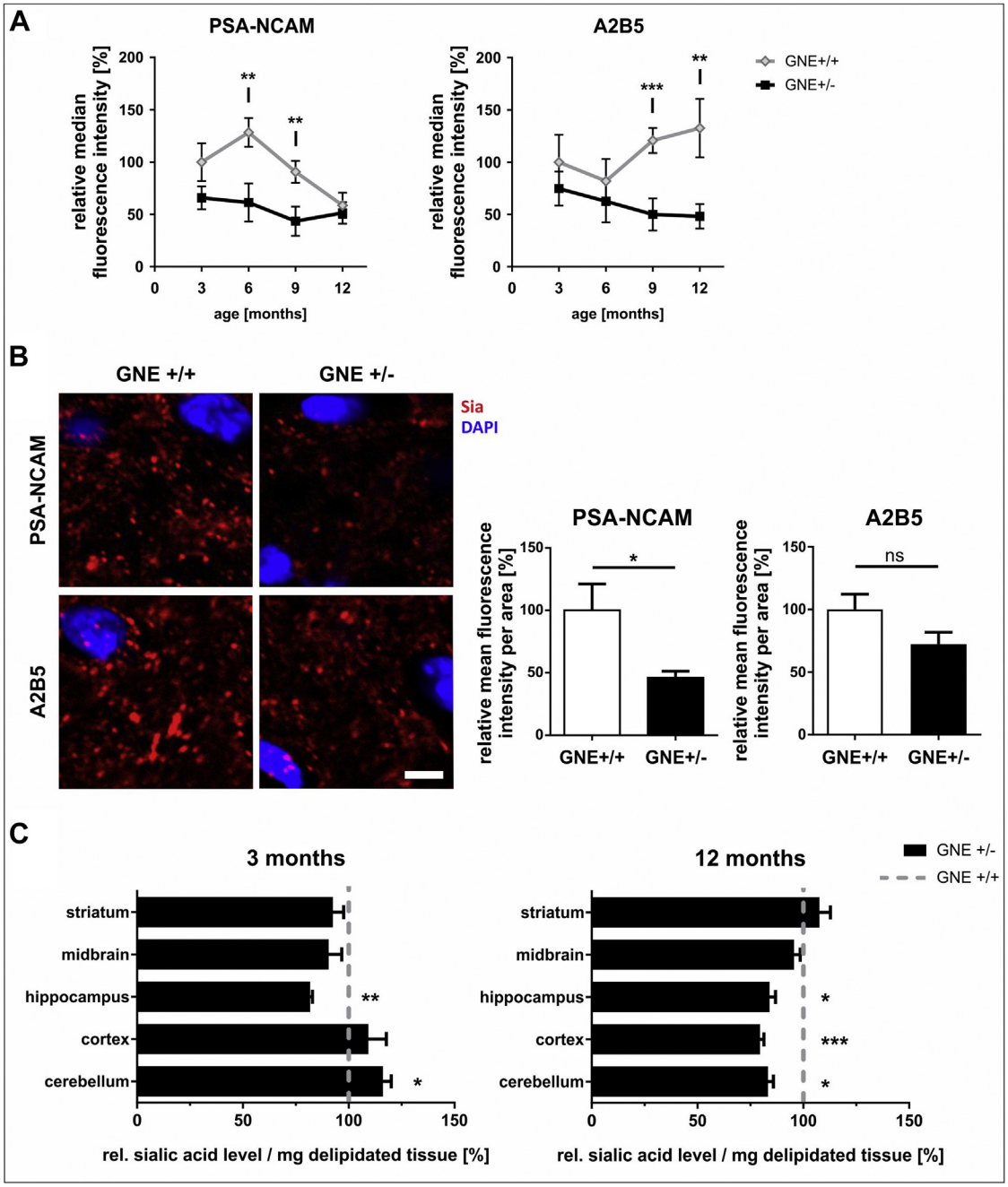

Fig. 1. Altered sialic acid biosynthesis in the brain of GNE+/− mice. (A) Flow cytometry of polysialylated neuronal cell adhesion molecule (PSA-NCAM) and the cell surface trisialic acid epitope A2B5 of gangliosides of GNE+/− and GNE+/+ mice. In wildtype (GNE+/+) mice, the median fluorescence intensity of long polymers of sialic acids (PSA-NCAM) decreased with age, while oligomers (A2B5) significantly increased. PSA-NCAM was decreased in GNE+/− mice at 6 and 9 months compared to GNE+/+ mice. A2B5 was decreased in GNE+/− mice at 9 and 12 months compared to GNE+/+ mice. Data are shown as mean ± SEM; normalized to 3 month old wildtype mice; n = 9–14 mice, pairwise comparison for GNE+/+ versus GNE+/− mice at different ages. (B) Left, Representative images of the hippocampus of 9 month old wildtype and GNE+/− mice at lateral sections between 1.30 mm and 1.40 mm. Sagittal brain slices were stained with the antibody PSA-NCAM (Sia; red) or A2B5 (Sia; red), and with the nuclear marker 4′,6-diamidino-2-phenylindole (DAPI; blue). Scale bar: 5 μm. Right, Quantification of the relative mean fluorescence intensity per area of the staining with PSA-NCAM or A2B5 revealed reduced polysialylation (PSA-NCAM) in GNE+/− mice compared to wildtype mice, while oligomers of sialic acids (A2B5) were less affected. Data shown as mean + SEM; normalized to wildtype levels; n = 7–8 mice. (C) Relative levels of protein-bound sialic acids differed between brain regions and were lower in the hippocampus but slightly higher in the cerebellum of 3 month old GNE+/− mice compared to wildtype littermates. In 12 month old mice, relative levels of protein-bound sialic acids were clearly reduced in hippocampus, cortex and cerebellum of GNE+/− mice. Data shown as mean + SEM relatively to GNE+/+ mice (=100%, gray dashed line); n = 4 mice. For all panels, ns = not significant, $^{*}p \leq 0.050$, $^{**}p \leq 0.010$, $^{***}p \leq 0.001$.

2.2. Increased loss of synapses and neurons in GNE+/− mice with aging

Polysialylation of NCAM is important for synaptic plasticity in the hippocampus and regulates neurotransmitter activity (reviewed in Sato and Kitajima, 2013). Furthermore, the CA3 region of the hippocampus is known for its susceptibility to seizures, stress and neurodegeneration (Cherubini and Miles, 2015). Therefore, sagittal sections of the hippocampus were analyzed by immunohistochemical staining with antibodies directed against the

neuronal nuclei (NeuN) marker and with the nucleus marker 4′,6-diamidino-2-phenylindole (DAPI). The relative cell density in the CA3 region was quantified at different time points to investigate the progression of the neuronal loss during aging (Fig. 2A, left). We found an age-related increase in neuronal loss in the CA3 region of GNE+/− mice. Neuronal cell density in the CA3 region of the hippocampus was almost identical between young GNE+/− and wildtype mice (≤6 months), but decreased faster in middle-aged GNE+/− mice (Fig. 2A, right; 3 months vs. 12 months, GNE+/−: -24.1%; $p < 0.001$) compared to their wildtype littermates (GNE+/+: −12.3%; $p = 0.030$). Finally, 12 month old GNE+/− mice had already 16% ($p = 0.005$) lower levels in cell density compared to wildtype mice at the same age.

To determine alterations in synaptic density that might precede the neuronal loss, we stained for the presynaptic marker vesicular glutamate transporter 1 (vGlut1) and the postsynaptic density (PSD) marker PSD95 in the hippocampus (Fig. 2B, left). Indeed, we found reduced levels of postsynaptic PSD95 puncta in the hippocampus of GNE+/− mice at 6 months (−69% vs. GNE+/+, $p < 0.001$; Fig. 2B, right). In line with these findings, the level of synapses as determined by colocalized vGlut1/PSD95 puncta was also decreased (−77% vs. GNE+/+, $p < 0.001$; Fig. 2B, right). Thus,

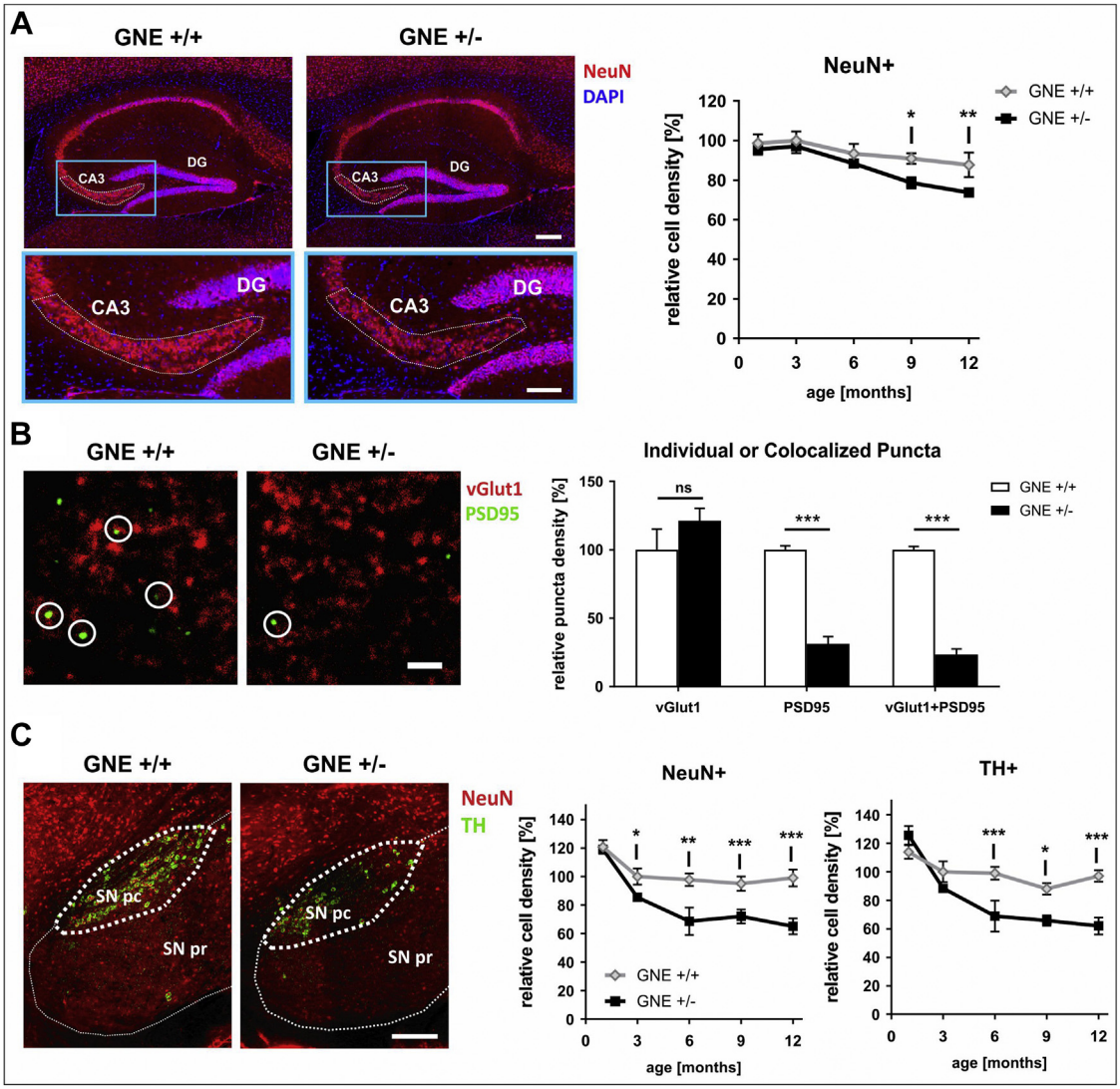

Fig. 2. Increased loss of synapses and neurons in GNE+/− mice with aging. (A) Left, Representative images of the hippocampus of 12 month old wildtype (GNE+/+) and GNE+/− mice at lateral sections between 1.10 mm and 1.20 mm. Lower images show a higher magnification of the analyzed CA3 region (white dotted line) of the hippocampus. Sagittal brain slices were stained with antibodies directed against neuronal nuclei (NeuN, red) and with 4′,6-diamidino-2-phenylindole (DAPI, blue). DG—dentate gyrus. Scale bar: 200 μm or 100 μm (higher magnification). Right, Quantification of the relative cell density of NeuN-positive cells showed higher neuronal loss in GNE+/− mice compared to wildtype littermates with increasing age. Data shown as mean ± SEM; normalized to 3 month old wildtype mice; n = 7–12 mice, pairwise comparison for GNE+/+ versus GNE+/− mice at different ages. (B) Left, Representative z-stack images of the hippocampus (dorsal of dentate gyrus) of 6 month old wildtype and GNE+/− mice at lateral sections between 1.20 mm and 1.30 mm stained with antibodies directed against vesicular glutamate transporter 1 (vGlut1; red) and postsynaptic density protein 95 (PSD95; green). White circles show colocalization (vGlut1+PSD95). Scale bar: 2 μm. Right, Quantification of the individual or colocalized synaptic puncta revealed a reduction in postsynapses in GNE+/− mice compared to wildtype littermates. Data shown as mean + SEM; normalized to wildtype levels; n = 4–6 mice. (C) Left, Representative images of the substantia nigra of 12 month old wildtype and GNE+/− mice at lateral sections between 1.10 mm and 1.20 mm. Sagittal brain slices were stained with antibodies against tyrosine hydroxylase (TH, green) and NeuN (red). SN pc—substantia nigra pars compacta, SN pr—substantia nigra pars reticulata. Scale bar: 200 μm. Right, Quantification of the cell density of NeuN- and TH-positive cells showed higher neuronal loss in GNE+/− mice compared to wildtype littermates with age. Data shown as mean ± SEM; normalized to 3 month old wildtype animals; n = 7–12 mice, pairwise comparison for GNE+/+ versus GNE+/− mice at different ages. For all panels, ns = not significant, $^{*}p \leq 0.050$, $^{**}p \leq 0.010$, $^{***}p \leq 0.001$.

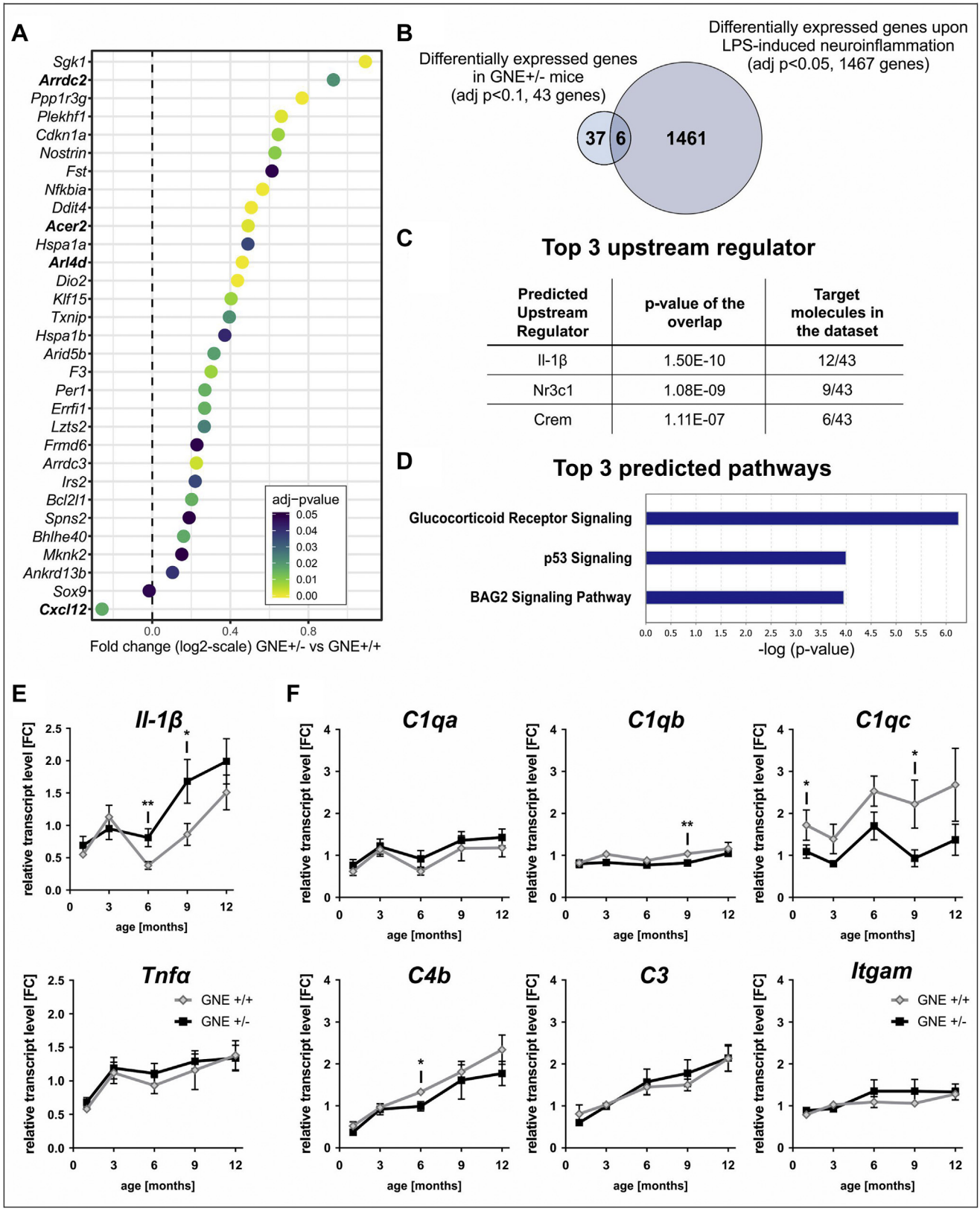

Fig. 3. Minor transcriptional changes in GNE+/− mice indicate homeostatic removal of synapses and neurons. RNA was isolated and sequenced from the brains of four 9 month old GNE+/− mice and 4 age-matched wildtype mice. (A) Snake plot of the most differentially expressed genes (DEGs) in GNE+/− mice compared to wildtype (GNE+/+) littermates with an adjusted *p*-value (adj *p*) of <0.05. Genes are ranked by fold change (log2-scale) and are color-coded for adj *p*. Most genes were upregulated. (B) Venn diagram comparing the total 43 DEGs (adj $p < 0.1$) with 1467 DEGs of brain samples upon systemic 4 × LPS-induced neuroinflammation (Bodea et al., 2014). Overlapping areas show the number of shared genes. Only 6 genes were shared. (C) Table of the top 3 predicted upstream molecules targeting most of the 43 DEGs. Il-1β - interleukin-1 beta; Nr3c1 – nuclear receptor subfamily 3 group C member 1; Crem - cAMP responsive element modulator. (D) Presentation of the top 3 canonical pathways enriched in the Ingenuity Pathway Analysis on the 43 significantly DEGs (false discovery rate, FDR <0.1). (E) Progression of Il-1β and tumor necrosis factor-α (Tnfα) transcription levels in the brains of 1 month to 12 month old mice. Il-1β levels are

synapse loss was preceding the accelerated neuronal loss in GNE+/− mice starting after 6 months.

Next, we investigated the neuronal density in another brain region. The substantia nigra is known for high levels of oxidative stress and susceptibility to neurodegeneration (Di Giovanni et al., 2012). Cells positive for the neuronal marker NeuN or the dopaminergic marker tyrosine hydroxylase (TH) were counted in the substantia nigra pars compacta (SN pc) to measure the relative cell density (Fig. 2C, left). In the SN pc of GNE+/− mice the neuronal cell density was decreased in 3 months and older mice compared to wildtype littermates (Fig. 2C, right). While the neuronal cell density stayed stable in wildtype mice over time (3 months vs. 12 months: 100.0 ± 5.6% vs. 98.9 ± 5.8%; $p = 0.889$), the levels decreased by 29.9% in GNE+/− mice from 3 months to 12 months (85.4 ± 2.7% vs. 65.0 ± 5.6%; $p = 0.002$; Fig. 2C, right). The density of TH-positive cells was decreasing by 23.9% from 3 months to 12 months (88.4 ± 2.4% vs. 62.0 ± 6.0%; $p = 0.001$) compared to wildtype littermates. However, the neuronal cell density of young GNE+/− mice was not affected. The cell densities were similar to wildtype levels at 1 month (NeuN: 119.0 ± 2.6% vs. 120.7 ± 4.8%; TH: 125.6 ± 6.5% vs. 113.8 ± 4.8%, GNE+/− vs. GNE+/+, respectively).

Thus, GNE+/− mice showed a decrease in neuronal density in the CA3 region of the hippocampus and in the SN pc compared to wildtype littermates during aging. In addition, reduced synaptic density was observed prior to the neuronal loss in the hippocampus.

2.3. Minor transcriptomic changes in GNE+/− mice

To better understand the underlying mechanisms that led to the observed accelerated age-related loss of synapses and neurons in the brain we performed a whole genome transcriptome analysis of 9 month old brain tissue from GNE+/− mice and wildtype littermates. After normalization of the RNA sequencing data, 47,643 separate genes were detected. Statistical comparison revealed only 31 significantly differently expressed genes (DEGs) with an adjusted p-value of <0.05 (Fig. 3A) and 44 significantly differently expressed genes with a less restricted adjusted p-value of <0.1, 43 of which correspond to experimentally confirmed mouse genes (Suppl. Table 2). Most of these 43 genes were upregulated in GNE+/− compared to wildtype mice and in total only 2 genes (*Cxcl12* and *Sox9*) were found to be downregulated. Many of the upregulated genes are transcription factors involved in apoptotic and metabolic pathways. We chose 3 upregulated genes involved in autophagy and the endosomal pathway, namely arrestin domain containing 2 (*Arrdc2*), alkaline ceramidase 2 (*Acer2*), ADP-ribosylation factor-like 4D (*Arl4d*), and the most significantly downregulated gene chemokine (C-X-C motif) ligand 12 (*Cxcl12*) and analyzed their levels by sqRT-PCR (Suppl. Fig. 4). The results obtained from the sqRT-PCR reflected the results from the RNA sequencing.

To understand whether the 43 genes could hint toward any underlying pro-inflammatory pathway that could explain neuronal loss, we compared these genes with genes found to be involved in the mechanism of inflammatory neurodegeneration as shown by Bodea and colleagues (Bodea et al., 2014). When we compared the 43 genes with the 1467 genes changing in this mouse model of inflammatory nigrostriatal neurodegeneration (Fig. 3B), we found only 6 overlapping genes (Suppl. Table 3). Thus, these data indicate that the GNE+/− mice do not show a typical pro-inflammatory transcriptome signature at 9 months that could explain the neuronal loss especially in the substantia nigra.

Using Ingenuity Pathway Analysis (IPA; Qiagen) on the 43 identified candidates we predicted interleukin-1β (Il-1β) as the most involved upstream regulator, followed by the nuclear receptor subfamily 3 group C member 1 (*Nr3c1*) encoding for glucocorticoid receptor (GR) and the cAMP responsive element modulator (*Crem*; Fig. 3C). Furthermore, the most significant canonical pathway involved was glucocorticoid receptor signaling (Fig. 3D). Glucocorticoid receptors, like GR, are intracellular messengers and directly or indirectly modulate the transcription of pro- and anti-inflammatory genes. In conclusion, the overall transcriptome analysis of brains at 9 months showed minor alterations, which are possibly related to Il-1β and glucocorticoid signaling.

To verify that there is no typical pro-inflammatory response, we performed a longitudinal gene transcript analysis by sqRT-PCR of brains of GNE+/− and wildtype mice at an age of 1 month, 3 months, 6 months, 9 months, and 12 months. We measured the transcription levels of the pro-inflammatory cytokines Il-1β and tumor necrosis factor alpha (Tnfα) as well as several factors of the complement system. We detected slightly elevated levels of the cytokine Il-1β in GNE+/− mice at 6 months and 9 months of age compared to wildtype littermates, but not at earlier time points (Fig. 3E). As expected, transcription levels of *Il-1β* were increased with age from 1 month to 12 months (GNE+/−: +130% vs. GNE+/+: +96%; both $p < 0.001$). Levels of *Tnfα* also showed an increase in transcription with age (1 month vs. 12 months; GNE+/−: +66% vs. GNE+/+: +80%; $p = 0.002$ and $p < 0.001$, respectively), but independent of the genotype (Fig. 3E). Similar to *Tnfα* levels we found an age- but not genotype-dependent increase for all analyzed components of the complement system, being highest for the complement components *C1qc*, *C4b,* and *C3* (Fig. 3F). The levels of *C1qc* were slightly reduced in GNE+/− mice ($p < 0.001$).

In summary, GNE+/− mice showed no classical signs of a strong pro-inflammatory component and only a minor up-regulation of *Il-1β* transcripts, in line with homeostatic innate immune functions of this cytokine.

2.4. Reduced arborization of microglia in GNE+/− mice during aging

Microglia, the yolk sac-derived brain macrophages, permanently monitor the brain parenchyma and sense small alterations that can lead to transcriptional and morphological changes. Sialylation on neurons might serve as an inhibitory flag for microglia (Linnartz et al., 2012; Wang and Neumann, 2010) and regulator of phagocytosis (Pluvinage et al., 2019). Therefore, we specifically measured the mRNA levels of the macrophage-/microglia-specific marker allograft inflammatory factor 1 (Aif1; the Iba1 encoding gene), the phagocytosis and activation marker Cd68 antigen (Cd68), and the microglia-specific marker transmembrane protein 119 (Tmem119) in brain homogenates of GNE+/− and wildtype mice at different ages (Fig. 4A). Minor genotype-specific effects were seen for *Aif1* ($p = 0.003$) and for *Tmem119* ($p = 0.040$), but not for *Cd68* ($p = 0.109$). From the age of 6 months onwards transcription levels of all 3 markers tended to be higher in GNE+/− mice compared to wildtype littermates.

increasing with age in both, GNE+/− and wildtype (GNE+/+) mice, but more significantly in GNE+/− mice. Data shown as mean ± SEM; normalized to 3 month old wildtype animals; n = 7–15 mice, pairwise comparison for GNE+/+ versus GNE+/− mice at different ages. (F) Progression of the transcription levels of the C1q subunits C1qa, C1qb, C1qc, of the complement components C4b, C3, and of a complement receptor 3 subunit (Itgam, integrin alpha M) in the brains from 1 month to 12 month old mice. Age-dependent upregulation was detectable for C4b and C3. Higher levels in GNE+/− mice were observed for C1qa, C3, and Itgam. Data shown as mean ± SEM; normalized to 3 month old wildtype animals; n = 7–15 mice, pairwise comparison for GNE+/+ versus GNE+/− mice at different ages. For all panels, ns = not significant, $^{*}p \leq 0.050$, $^{**}p \leq 0.010$.

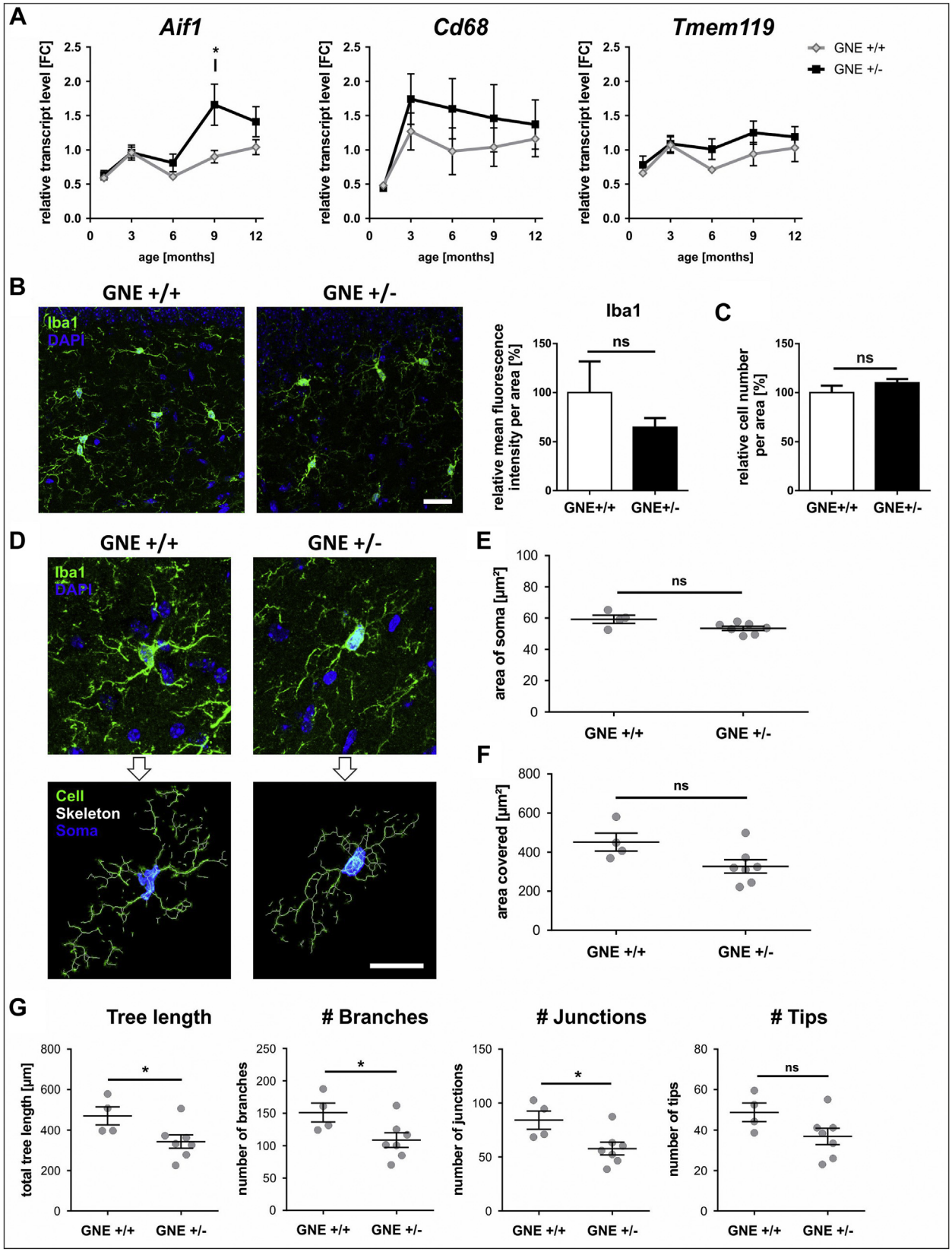

Fig. 4. Reduced arborization of microglia in GNE+/− mice during aging. (A) Transcription levels of allograft inflammatory factor 1 (Aif1; gene of Iba1), the CD68 antigen (Cd68), and the transmembrane protein 119 (Tmem119) of whole brain homogenates from 1 month until 12 month old mice tended to be higher in GNE+/− mice from 6 months onward. Data shown as mean ± SEM; normalized to 3 month old wildtype (GNE+/+) animals; n = 7–15 mice, pairwise comparison for GNE+/+ versus GNE+/− mice at different ages. (B) Left, Representative z-stack images of microglia in the hippocampus (dorsal of dentate gyrus) of 6 month old GNE+/− mice and wildtype littermates at lateral sections of ~1.30 mm. Sagittal brain slices were stained with antibodies directed against the microglial marker ionized calcium binding adaptor molecule 1 (Iba1; green) and with the nucleus marker 4′,6-diamidino-2-phenylindole (DAPI; blue). Scale bar: 25 µm. Right, Quantification of the relative Iba1 fluorescence intensity per area revealed a trend to lower levels in GNE+/− mice.

Next, we analyzed the Iba1 intensity of immunostained microglia from brain sections of 6 month old GNE+/− and wildtype mice. GNE+/− mice showed a tendentially reduced Iba1 protein expression in the hippocampus (Fig. 4B), but no difference in the number of Iba1-positive cell bodies (Fig. 4C). Interestingly, images indicated a slightly different morphological appearance of microglia with less branches in GNE+/− mice that could explain the reduced overall Iba1 protein expression.

To elucidate possible alterations in microglial morphology in more detail, we quantified microglial morphology in the hippocampus of 6 month old mice. Sections stained with an antibody directed against the microglial receptor Iba1 and with the nuclear stain DAPI were used to reconstruct the microglia skeleton in z-stacks (Fig. 4D). At least 6 microglial cells were reconstructed per mouse (Single-cell data: Suppl. Fig. 5). We found no differences in the soma size of microglia from GNE+/− mice compared to wildtype littermates at 6 months (Fig. 4E).

However, microglia from GNE+/− mice covered a smaller area (327.2 ± 34.4 μm vs. 451.4 ± 46.1 μm in GNE+/+; $p = 0.058$; Fig. 4F). Furthermore, the total tree length of microglial processes was reduced from an average of 470.0 ± 44.8 to 343.3 ± 33.2 ($p = 0.048$) in GNE+/− mice. Additionally, microglia from GNE+/− mice showed less branches, junctions, and tips compared to wildtype mice (Fig. 4G). In detail, microglia of GNE+/− mice at 6 months showed a reduction in the number of branches from 151.0 ± 14.6 to 108.6 ± 11.3 ($p = 0.048$) and in the number of junctions from 84.2 ± 8.5 to 57.9 ± 5.8 ($p = 0.028$). The total number of branch tips tended to decline from 48.8 ± 4.6 to 36.9 ± 4.1 ($p = 0.098$; Fig. 4G).

Altogether, differences in the transcription levels of microglial markers were minor with a very slight increase of *Aif1* in GNE+/− mice at 9 months. However, quantifying microglial morphology revealed a reduction in branches, junctions, and total process length at 6 months in GNE+/− mice. The reduced microglial arborization was coinciding with an overall decreased hippocampal Iba1 protein expression in 6 month old GNE+/− mice.

2.5. Transcriptome analysis of crossings between GNE+/− mice and C3−/− mice

Complement-mediated remodeling of neurons by microglia is known from brain development (Paolicelli et al., 2011; Schafer et al., 2012). Microglia can actively engulf synaptic structures, and thereby, contribute to the regulation of neuronal connectivity. To analyze whether the in vivo observed loss of synapses and neurons is dependent on the activation of the complement cascade, GNE+/− mice were crossbred with mice deficient for the central complement component C3. The deletion of the *C3* gene was confirmed on transcription level in the brain of 9 month old mice and did not affect *Gne* transcript levels (Suppl. Fig. 6). Again, a whole genome transcriptome analysis was performed to compare all 4 groups (GNE+/+C3+/+ = wildtype, GNE+/−C3+/+, GNE+/+C3−/− and GNE+/−C3−/−; for the lists of all 3 contrasts see supplementary data).

The principle component analysis of the brain transcriptome at 9 months revealed that *C3*-deficiency had a much higher impact on gene transcription than *Gne*-heterozygosity (Fig. 5A). The sample group wildtype versus GNE+/−C3−/− had 981 DEGs compared to the above-described 43 genes that were differentially expressed in the wildtype versus GNE+/−C3+/+ group (Fig. 5B). In summary, differential expression of only 11 genes in GNE+/−C3+/+ mice was abolished by *C3*-deficiency, out of which 8 genes were specific to GNE+/−C3+/+ and were partially or fully corrected to wildtype levels in GNE+/−C3−/− mice (Suppl. Table 4). Three genes that returned closer to the wildtype group in GNE+/−C3−/− mice were dysregulated in both, GNE+/−C3+/+ and GNE+/+C3−/− mice (Suppl. Table 5). These findings were in line with brain transcription levels in 9 month old mice, determined by sqRT-PCR (Fig. 5C).

The innate immune markers *Il-1β* (Fig. 5D), complement component *C1qb* and *Itgam* (Fig. 5E), all altered in GNE+/−C3+/+ mice, showed a tendency to be rescued in *C3*-deficiency. In addition, the transcript level of the microglial marker *Aif1* increased in GNE+/−C3+/+ mice, was completely rescued under *C3*-deficiency (Fig. 5F). In line with these transcript level findings, also alterations in microglia morphology were less pronounced under *C3*-deficiency. Reconstructing Iba1-immunostained microglia in GNE+/−C3−/− and GNE+/+C3−/− mice demonstrated a neutralizing effect of reduced sialic acid on the partial loss of arborization (Fig. 5G). The area covered by microglia of GNE+/−C3−/− mice was similar to GNE+/+C3−/− (Fig. 5H) and the tree length, branches, junctions, and tips were almost at comparable levels in GNE+/− mice under *C3*-deficiency (Fig. 5I). In detail, in 6 month old GNE+/−C3−/− mice microglia covered 94% ± 0.1% of the area of microglia of GNE+/+C3−/− mice, revealed 91% ± 0.1% of the tree length of GNE+/+C3−/− microglia and 93% ± 0.1%, 94% ± 0.1%, and 90% ± 0.0% of the number of branches, junctions and tips of microglia from GNE+/+C3−/− mice, respectively (Fig. 5I).

Thus, data demonstrate a partial rescue of altered gene transcripts after backcrossing of the GNE+/− mice into C3−/− mice, indicating a return to a more healthy status in a *C3*-deficient situation. More importantly, the reduction of microglial arborization in GNE+/- mice was almost completely neutralized in *C3*-deficient mice, hinting to an involvement of microglial cells in the GNE+/− phenotype.

2.6. The complement system as key player in removal of synapses and neurons in GNE+/− mice

Whole genome transcriptome data and microglial morphological analysis indicate a possible rescue of the GNE+/− phenotype upon *C3*-deficiency. To clarify the effect of the complement system on the neuronal density, immunohistochemical stainings of 12 month old mice were performed in *C3*-deficient mice. Quantification of the NeuN-positive cells in the CA3 region of the hippocampus revealed a rescue in neuronal density (Fig. 6A). The reduced neuronal density present in GNE+/−C3+/+ mice compared to wildtype (−16%; $p = 0.045$) was not detected in GNE+/−C3−/− mice ($p = 0.003$ vs. GNE+/−C3+/+). The neuronal density in the CA3 region of GNE+/−C3−/− mice was similar to the levels of wildtype and GNE+/+C3−/− mice (104.3 + 3.0% vs. 100.0 + 9.3% and vs. 96.9 + 2.6%, respectively; all $p = 1.000$).

Data shown as mean + SEM; n = 6–7 mice; Student's t-test. (C) Quantification of the relative microglial (Iba1+/DAPI+) cell density showed no differences. Data shown as mean + SEM; n = 6–7 mice; Student's t-test. (D) Up, Maximum intensity projections of confocal z-stack images illustrating the microglial morphology in sagittal sections of the hippocampus from 6 month old GNE+/− mice and wildtype littermates and Below, Iba1-based 2D reconstruction of the cell (green), the cell skeleton (white), and the soma (blue) of the respective microglial cell from wildtype and GNE+/− mice. Scale bar: 20 μm. (E) Quantitative analysis of the soma area of microglia from wildtype mice in comparison to microglia from GNE+/− mice revealed no differences. Data shown as mean ± SEM; n = 4–7 mice; Student's t-test. (F) Quantitative analysis of the 2D reconstruction of microglia from GNE+/− mice showed a clear tendency in reduction of the area covered by each cell compared to wildtype littermates ($p = 0.058$). Data shown as mean ± SEM; n = 4–7 mice; Student's t-test. (G) Quantitative analysis of total tree length, number of cell branches, number of cell process junctions, and number of cell branch tips of microglia from GNE+/− mice revealed a lower arborization in GNE+/− compared to wildtype mice. Data shown as mean ± SEM; n = 4–7 mice; Student's t-test. For all panels, ns = not significant, $^{*}p \leq 0.050$.

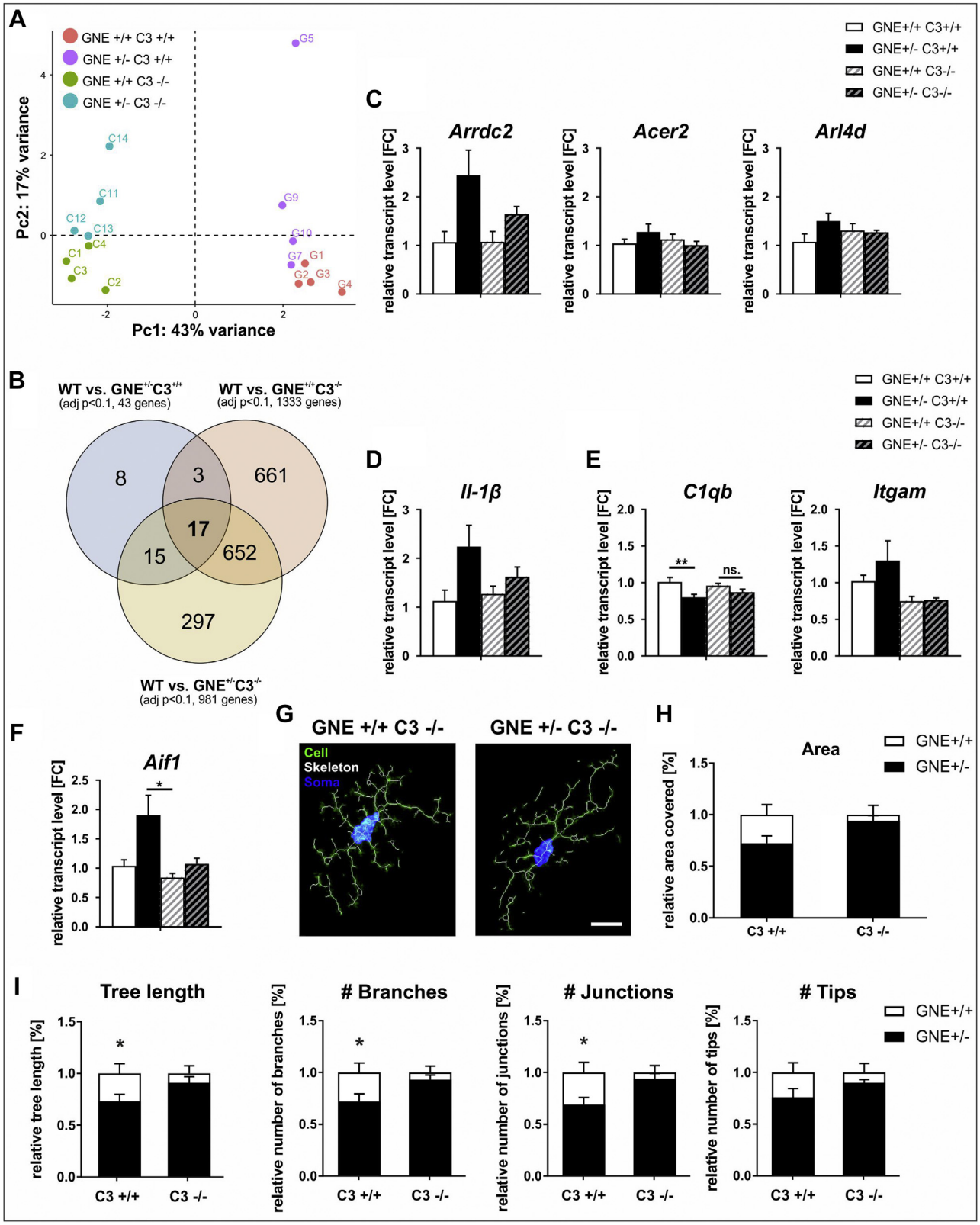

Fig. 5. Complement component 3 (C3)-deficiency partially rescues altered gene transcription in the brain of GNE+/− mice. GNE+/− mice were crossbred with C3-deficient mice and RNA was isolated and sequenced from brains of 9 month old mice of all 4 groups. (A) Principle component (PC) analysis of all 4 RNA-seq data sets represented by a color code. Each dot represents one brain transcriptome. Dashed lines indicate zero for both x- and y-axis. n = 4 mice. (B) Venn diagram of the differentially expressed genes (DEGs; adj $p < 0.1$) in each genotype group (WT = GNE+/+C3+/+). Overlapping areas show the number of shared genes. n = 4 mice. (C–F) Transcript levels of the selected genes arrestin domain containing 2 (Arrdc2), alkaline ceramidase 2 (Acer2), ADP-ribosylation factor-like 4D (Arl4d; all C), the cytokine interleukin-1 beta (Il-1β; D), the complement component C1qb as well as the subunit of complement receptor 3 (Itgam, integrin alpha M; both E) and the microglia marker allograft inflammatory factor 1 (Aif1, gene of Iba1; F), were measured in brain homogenates from 9 month old GNE+/+C3−/− and GNE+/−C3−/− mice and compared to wildtype (GNE+/+C3+/+) mice. Almost no Gne-dependent differences were present in C3-deficient mice. Data shown as mean + SEM; normalized to 9 month old wildtype mice. n = 4–14 mice; one-way ANOVA with Bonferroni or Dunnett's T3 post hoc

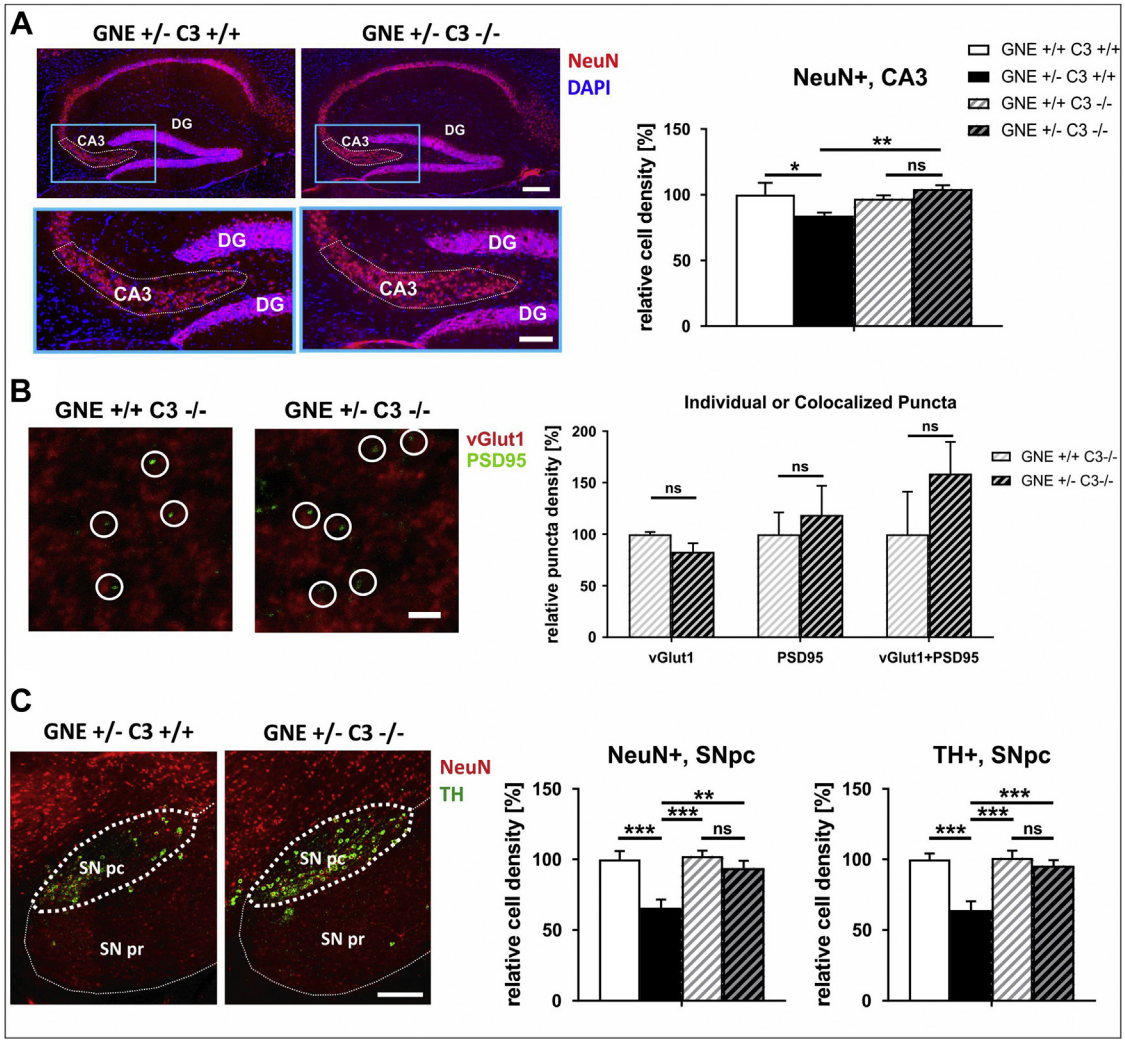

Fig. 6. The complement system as key player of homeostatic synapse and neuron removal. GNE+/− mice were crossbred with complement C3-deficient mice and were analyzed at 6 months or 12 months. (A) Left, Representative images of the CA3 region (white dotted line) stained for neuronal nuclei (NeuN; red) and cell nuclei (DAPI; blue) in the hippocampus of 12 month old GNE+/−C3+/+ and GNE+/−C3−/− mice. Scale bar: 200 μm or 100 μm (higher magnification). DG—dentate gyrus. Right, Quantification of the cell density of NeuN-positive cells in the CA3 region of 12 month old wildtype and GNE+/− mice revealed a complete rescue of neuronal cell density loss by C3-deficiency. Data shown as mean + SEM; normalized to 12 month old wildtype animals; n = 10–13 mice, one-way ANOVA with Bonferroni post hoc correction. (B) Left, Representative images of the hippocampus (dorsal of dentate gyrus) of 6 month old GNE+/+C3−/− and GNE+/−C3−/− mice at lateral sections between 1.20 mm and 1.30 mm stained with antibodies directed against the presynaptic marker vesicular glutamate transporter 1 (vGlut1; red) and the postsynaptic density protein 95 (PSD95; green). White circles show colocalization (vGlut1+PSD95). Scale bar: 2 μm. Right, Quantification of the density of individual or colocalized synaptic puncta of vGlut1 and PSD95 in the hippocampus of 6 month old GNE+/+C3−/− mice compared to GNE+/−C3−/− mice is shown. Loss of synapses was absent in C3-deficient mice. Data shown as mean + SEM; n = 3–6 mice; Student's t-test. (C) Left, Representative images of the substantia nigra of 12 month old GNE+/−C3+/+ and GNE+/−C3−/− mice stained with antibodies directed against tyrosine hydroxylase (TH, green) and neuronal nuclei (NeuN, red). SN pc—substantia nigra pars compacta, SN pr—substantia nigra pars reticulata. Scale bar: 200 μm. Right, Quantification of the cell density of NeuN- (left graph) and TH-positive cells (right graph) in the SN pc of 12 month old mice revealed almost a complete rescue of the GNE+/−dependent neuronal loss. Data shown as mean + SEM; normalized to 12 month old wildtype animals; n = 9–13 mice, one-way ANOVA with Bonferroni post hoc correction. For all panels, ns = not significant, $^{*}p \leq 0.050$, $^{**}p \leq 0.010$, $^{***}p \leq 0.001$.

Next, we also analyzed pre- and postsynaptic puncta in the hippocampus of GNE+/−C3−/− and GNE+/+C3−/− mice at 6 months by immunohistochemical staining and could not find any significant differences in density (Fig. 6B). The density of colocalized puncta around the dentate gyrus was even slightly higher in GNE+/−C3−/− compared to GNE+/+C3−/− mice. In detail, in the hippocampus the mean individual vGlut1 puncta differed from 100.0 + 2.1% in GNE+/+C3−/− mice to 77.3 + 11.5% in GNE+/−C3−/− mice, the mean PSD95 puncta from 100.0 + 26.5% to 118.4 + 36.5% and the mean colocalized puncta from 100.0 + 49.1% to 147.2 + 36.6%, respectively.

Even the loss of neurons in the SN pc of GNE+/−C3+/+ mice (−34%; $p \leq 0.001$ vs. wildtype) was not present in 12 month old GNE+/−C3−/− mice as shown by immunohistochemical staining of NeuN and TH (Fig. 6C, left). The neuronal cell density of GNE+/−C3−/− mice (93.8 + 5.2%) reached almost the same levels

correction. (G) Iba1-based reconstruction of the cell (green), the cell skeleton (white), and the soma (blue) of representative microglial cells from 6 month old GNE+/+C3−/− and GNE+/−C3−/− mice. Scale bar: 20 μm. (H) Quantitative analysis of the reconstruction of microglia from GNE+/+C3−/− and GNE+/−C3−/− mice were set in comparison to GNE+/+ (equals 1) and GNE+/− mice to show the rescue effect. Data shown as mean + SEM; n = 3–7 mice; Student's test. (I) Quantitative analysis of total tree length, number of cell branches, number of cell process junctions, and number of cell branch tips of microglia from GNE+/+C3−/− (equals 1) and GNE+/−C3−/− mice were set in comparison to GNE+/+ (equals 1) and GNE+/− mice. Differences diminished under C3-deficiency. Data shown as mean + SEM; n = 3–7 mice; Student's test. For all panels, ns = not significant, $^{*}p \leq 0.050$, $^{**}p \leq 0.010$.

as those of wildtype mice (100.0 + 5.9%) and of GNE+/+C3−/− mice (103.6 + 4.6%; both $p = 1.000$ vs. GNE+/−C3−/−) compared to GNE+/−C3+/+ mice (65.8 + 5.7%; $p = 0.002$ vs. GNE+/−C3−/−; Fig. 6C, left graph). The same rescue-effect was seen for the dopaminergic cell density in the SN pc (Fig. 6C, right graph). While in GNE+/−C3+/+ mice the relative cell density of TH-positive cells was at 64.1 + 6.2% compared to 100.0 + 4.2% in wildtype mice (−34%; $p \leq 0.001$), the cell density was similar to wildtype levels in *C3*-deficient mice (GNE+/−C3−/−: 95.5 + 4.1%, GNE+/+C3−/−: 104.2 + 5.7%; both $p = 1.000$ vs. GNE+/+C3+/+).

Taken together, *C3*-deficiency prevented the increased loss of synapses at 6 months and the subsequent neuronal loss at later time points in the hippocampus and the SN pc of GNE+/− mice. Thus, data indicate the complement system as being the driving force in neuronal loss upon insufficient sialylation in the GNE+/− mice.

3. Discussion

Microglia fulfill an important role in brain homeostasis that also involves phagocytic clearance of supernumerous synapses and axons during development. This microglia-neuron crosstalk has been shown to be mediated via soluble components of the classical complement system (C1q, C3) and TYROBP-activation signaling receptors (CR3, TREM2) on microglia (Filipello et al., 2018; Schafer et al., 2012; Stevens et al., 2007). Our data now suggest that sialic acids as the terminal cap of the glycocalyx act as an additional structure to regulate brain homeostasis in conjunction with complement component 3 (C3). Reduced sialic acid levels could act as a trigger for an age-related and complement C3-dependent loss of synapses and neurons.

Sialic acids are nine-carbon sugars that can build linear saccharides of different length like mono-, di-, tri-, oligo- and polysialic acids. Most of the oligo- and polysialic acids are bound to membranes with a huge variety of biological functions. Sialic acids are known to reflect the cellular health's status (Rachmilewitz, 2010) and are sensed by the inhibitory microglial Siglec receptors as well as the complement factor H (Blaum et al., 2015; Crocker et al., 2007). In mammals, the central nervous system is the organ with the highest sialic acid expression level (Schnaar et al., 2014). During brain development, sialic acid levels are increased by local cellular production and incorporation of exogenous sialic acids during breast feeding, while in the aging brain sialic acid levels of gangliosides are continuously decreasing (Svennerholm, 1994; Svennerholm et al., 1997, 1989). This dynamic of sialic acid expression has already been observed 1983 in rats using the example of polysialic acids that are present on NCAM (Margolis and Margolis, 1983): The concentration of polysialylated glycopeptides decreased by about 75% within the first month after birth. While in newborn rats (day 1) 30% polysialylation was measured, the amount of polysialylated glycopeptides decreased over 14% at day 6 to 4% at day 28 of age (Margolis and Margolis, 1983).

Desialylation, the removal of sialic acids by endogenous or bacterial neuraminidases as well as oxidation processes, leads to the exposure of underlying structures that can be recognized by the complement system or phagocytic receptors resulting in complement attack or phagocytosis (Wei and Wang, 2019). Heterozygous GNE mice (GNE+/−) mimic this situation of having less sialic acids on the cell surface since these mice show a reduction of ~32% of membrane-bound sialic acids in the brain (Gagiannis et al., 2007). We confirmed a slightly reduced expression of total protein-bound sialic acids in GNE+/− mice and showed that especially the presence of polysialic acid chains and trisialic acid were reduced in GNE+/− mice. Interestingly, decrease of protein-bound sialic acids during aging of rats has also been observed on erythrocytes, an effect that has been postulated to reflect a biomarker of the aging process (Kumar and Rizvi, 2013). Reduced levels of polysialic acid were also found in a study of human Alzheimer's disease postmortem tissue using immunohistochemical stainings with 2 different polysialic acid specific antibodies (clones 5A5 and 2-2B; Murray et al., 2016). In addition, an accentuated decrease of polysialic acids was found in the entorhinal cortex of postmortem human brain tissue that inversely correlated with tau load (Murray et al., 2016).

Our data now demonstrate enhanced neuronal loss during aging in the 2 analyzed brain regions, hippocampus CA3 and SNpc, of GNE+/− mice. Whether other brain regions are affected as well has not been investigated within this study. Worth to mention, the neuronal loss was not yet present in 1 month old mice, suggesting that the loss is unlikely to be a developmental phenotype. It rather is an age-related effect with synaptic loss as one of the first pathological signs. Loss of synapses is a process that often precedes the neuronal loss in several neurodegenerative disease. Consequently, the loss of neuronal density will become more visible the older the mice grow. Thus, slightly reduced sialic acid levels with a significant reduction in oligo- and polysialylation as observed in GNE+/− mice could be interpreted as one possible trigger of accelerated aging, mediated via complement C3-dependent loss of synapses and neurons.

GNE+/− mice do not develop signs of myopathy (Gagiannis et al., 2007), while loss-of-function mutations in the GNE gene have been described in humans causing GNE-related myopathy (Hereditary Inclusion Body Myopathy - HIBM2) with hyposialylation of skeletal muscles. The onset of symptoms in GNE-related myopathy starts in late teenage years or early adulthood and leads to wheelchair-bound patients. Intellectual abilities appear to be unaffected (reviewed in O'Ferrall and Sinnreich, 1993). However, to our knowledge it has not been investigated whether GNE-related myopathy patients might have a higher risk to develop a cognitive decline at advanced age (see also orphanet, ORPHA:602 and current review Pogoryelova et al., 2018). Interestingly, patients of a family with a mutation in another key enzyme in sialic acid synthases, namely a homozygous mutation in CMAS, show intellectual disability (Qu et al., 2019).

Terminal sialic acids are also present on most gangliosides. Interestingly, mutations in several of the enzymes involved in synthesizing the different types of gangliosides result in cognitive decline in human patients and diverse mouse models (Boukhris et al., 2013; Simpson et al., 2004; Yamashita et al., 2005). Also mice displaying less polysialic acids such as mice deficient for the polysialyltransferase ST8SiaIV/PST-1 show deficits in learning and memory formation (Cremer et al., 1994; Eckhardt et al., 2000), but to our knowledge age-related neurodegeneration was not analyzed in these mice. Thus, our data in conjunction with the neuronal phenotypes described in gangliosides and polysialic acid-deficient mice strengthen an important role for intact sialylation as a neuroprotective factor during aging.

Functional in vitro studies indicated that sialylation might prevent the binding of activators of the complement system and the uptake of neuronal target structures by microglia or macrophage phagocytosis in mice and humans (Linnartz et al., 2012; Linnartz-Gerlach et al., 2016). It was postulated that sialic acids regulate the binding of C1q to neurons and the subsequent removal of neuronal structures by microglia in a complement-receptor 3-dependent manner (Linnartz et al., 2012; Linnartz-Gerlach et al., 2016). In line with these initial in vitro data, GNE+/− mice with reduced levels of sialic acids showed also progressive loss of neurons with different degrees of severity for the different brain regions.

Sialic acids are involved in a variety of biological functions and molecular interactions. They are highly anionic and are cleaved from the underlying proteins or lipids by specific neuraminidases, mainly within the lysosomes, but also on the cell membrane. Thus, decreased membrane-bound sialic acid levels principally might have direct effects on lysosomal function without affecting gene transcript levels.

Surprisingly, the neuronal loss seen in GNE+/− mice was not accompanied by a typical pro-inflammatory signature that often accompanies prototypic inflammatory neurodegenerative diseases. Comparing the transcriptomic dataset obtained in this study with the transcriptome analysis of a brain with repeated, systemic LPS-triggered inflammatory neurodegeneration revealed a clear difference in the pro-inflammatory profile between loss of neurons in GNE+/− mice and LPS-triggered nigrostriatal neurodegeneration. Thus, the underlying mechanism seems to be rather silent phagocytosis of desialylated neuronal structures, possibly a non-inflammatory, but homeostatic innate immune system related removal process. In accordance with a non-inflammatory mechanism, astrogliosis was absent in the GNE+/− mice. Only, Il-1β, an innate immune cytokine released by microglia that is also well known for a number of homeostatic functions (Blatteis and Sehic, 1998; De Castro E Silva et al., 2006; Ingiosi et al., 2015; Luz et al., 2006, 2009; Morimoto et al., 1986; Netea et al., 2000), was found to be a predicted upstream regulator in the transcriptomic analysis. It was confirmed to be transcribed in higher levels in GNE+/− mice from 6 months on. Likewise, in mouse models with loss of gangliosides Il-1β has been shown to be upregulated simultaneously with loss of neurons (Ohmi et al., 2014, 2011) and the authors demonstrated that the complement system plays a major role in the neuronal loss. Furthermore, mating with *C3*-deficient mice was able to restore the negative effects of ganglioside alterations.

Furthermore, the glucocorticoid signaling pathway was the first hit among the canonical pathways altered in GNE+/− mice. Glucocorticoids act as counterparts to Il-1β and are response hormones to acute stress signals (reviewed in (Hall et al., 2015). Lately, glucocorticoids were also found to be involved in synaptic plasticity. Endogenous glucocorticoid oscillations promoted spine formations and were required for spine stabilization (Liston et al., 2013), whereas chronic excessive glucocorticoid signaling due to stress eliminated new spines (Sousa et al., 2000).

During development, the microglial TYROBP-signaling receptors triggering receptor expressed on myeloid cells 2 (TREM2) and complement receptor 3 (CR3), as well as the complement components C1q and C3 can mediate synaptic pruning and the maturation of the neuronal network (Filipello et al., 2018; Kraft et al., 2016; Schafer and Stevens, 2010; Stevens et al., 2007), but the exact target structures of the complement binding on the neurons remain unclear. By crossbreeding the GNE+/− mice with *C3*-deficient mice, synapse loss, neuronal loss as well as the slight but not significant upregulation of Il-1β and the significant upregulation of the microglial marker Aif1/Iba1 were rescued in our study, demonstrating that the complement system plays an essential role in loss of neurons. A similar rescue observation was made previously in a mouse model of ganglioside deficiency, in which the loss of spinal cord neurons of double knockout mice of ganglioside GM2/GD2 synthase (B4GANLT1) and GD3 synthase (ST8SIA1) was rescued by crossbreeding with *C3*-deficient mice (Ohmi et al., 2014, 2011). Furthermore, it was recently demonstrated in mice with deficiency of the sialic acid-activating enzyme CMP-sialic acid synthase (CMAS) that sialic acid is a critical protective component against maternal complement attack during embryonic development in mice (Abeln et al., 2018).

Thus, reduced masking of the glycocalyx by sialic acids and possible exposure of underlying aminophospholipids might be one possible explanation for increased complement binding and complement-mediated synapse elimination by microglia followed by neuronal loss in chronic neurodegenerative diseases and aging.

In summary, GNE+/− mice might mimic a natural overall decline in polysialic and oligosialic acid levels with aging and display a slow increase in age-related and complement-dependent neuronal loss. Thus, the results obtained in this study indicate that the polysialic and/or oligosialic acid expression of the glycocalyx plays an essential role in maintaining brain homeostasis in vivo and is an important underestimated recognition system for the innate immune system with possible relevance in aging and neurodegeneration.

4. Material and methods

4.1. Mice

All mouse experiments have been approved by the authors' institutional review boards and by the local government and have been conducted according to the principles expressed in the Declaration of Helsinki. We used C57BL/6J mice, mice heterozygous for the enzyme UDP-N-acetylglucosamine-2-epimerase/N-acetylmannosamine kinase (GNE; (Schwarzkopf et al., 2002)) backcrossed for at least 10 generations with C57BL/6J mice in our facilities (referred hereafter as GNE+/− mice), and B6; 129S4-C3tm1Crr/J backcrossed for at least 8 generations into C57BL/6J (referred hereafter as C3−/− mice) that were obtained from the Jackson Laboratory via Charles River (Rathcoole-Dublin, Ireland). To reduce gender-specific variability, only female mice were used for sialic acid determination, flow cytometry, and RNA sequencing, whereas only male mice were used for sqRT-PCR and immunohistochemistry. For tissue collection mice were anesthetized by intraperitoneal injections (200 mg/kg Ketamin + 40 mg/kg Xylazin) and perfused transcardially with cold saline at the desired age.

4.2. Flow cytometry analysis of GNE+/− mice brain tissue

Whole brain was harvested of PBS perfused mice, directly homogenized manually through a 70 μm cell strainer and washed with cold saline. The cell suspension was centrifuged for 3 minutes at 1500 rpm and post-fixed with 4% paraformaldehyde (PFA; Sigma-Aldrich, Taufkirchen, Germany) for 10 minutes on ice. The cells were washed twice with cold saline and subsequently incubated in blocking solution (10% bovine serum albumin [BSA; Sigma-Aldrich, Germany] + 0.1% Triton X-100 [Sigma-Aldrich, Germany] + 5% normal goat serum [NGS; Invitrogen/Thermo Fisher Scientific, Schwerte, Germany] in PBS) for one hour on ice. Fixed cells were resuspended in cold saline, separated into equal samples, and incubated with primary antibodies (2.5 μg/mL) against polysialylated neuronal cell adhesion molecule (PSA-NCAM; clone: 2-2B; Millipore MAB5324, Darmstadt, Germany) and A2B5 (clone: 105; BD Biosciences #563775, Heidelberg, Germany), and their respective isotype controls (all from BD Biosciences) for one hour on ice. After washing twice, the cells were stained with the respective PE-coated secondary antibodies (all from Jackson Immuno Research/Dianova, Hamburg, Germany) for 30 minutes on ice in the dark. Cells were washed twice and were resuspended in 500 μL cold saline for flow cytometry analysis. For each mouse one sample was kept on ice without any staining (blank sample; suppl. Fig. 2A). Analysis was done with a FACS Calibur flow cytometer and FlowJo Software (both BD Biosciences). The intact cell population was gated first in a blank sample and then in an isotype control for PE-positive staining (suppl. Fig. 2A and B). The median fluorescence of each sample was measured and normalized to 3 month old wildtype mice.

4.3. Sialic acid determination by high-performance liquid chromatography (HPLC) analysis

Peripheral organs (spleen, right kidney, liver lobe) and brain were collected from PBS perfused mice. The brain was directly dissected on ice and the following parts were collected: striatum, midbrain, hippocampus, cortex, cerebellum. Tissue was shock-frozen on dry ice and stored at −80 °C until usage. Tissue samples were homogenized and delipidated according to the Folch method (Folch et al., 1957). Briefly, tissues were homogenized in 1 mL of chloroform/methanol (2:1) using pellet pestles (Sigma-Aldrich, Hamburg, Germany). The whole mixture was agitated in the shaker for 20 minutes; followed by centrifugation at 13,000 × g for 30 minutes. Homogenized pellet was suspended in water and treated with an equal volume of 4 M propionic acid (end concentration: 2 M) for 4 hours at 80 °C with gentle shaking. After cooling on ice, the hydrolyzed samples were lyophilized using the Finn Aqua GT2 lyophilizer (Bemini Bv, Apeldoorn, The Netherlands). Dried samples were mixed with 2 mL of sterilized water, and anion exchange column purification was performed. For the purification step 1 mL AG 1X8 HCOO- 200–400 meshes (BioRad, Munich, Germany) was used. Samples were passed through the columns, followed by a 5×-column-volume of sterilized water. Sialic acid was eluted with a 5×-column-volume of 2 M propionic acid, and again washed with a 5×-column-volume of sterilized water. Both, the acid eluate and the final water wash eluate were mixed, freeze-dried and used for labeling with 1,2-diamino-4,5-methylenoxybenzene (DMB; Sigma-Aldrich, Hamburg, Germany). 50 μL of DMB and 50 μL of sample were mixed and incubated at 56 °C for 60 minutes. Samples were cooled on ice, followed by HPLC analysis using the Shimadzu pump-LC-20AT (Shimadzu, Canby, Oregon, USA). A volume of 10 μL–20 μL of labeled samples were injected in the reversed phase C18 column (Merck, Darmstadt, Germany) and the elution was performed with the isocratic solvent acetonitrile/methanol/water (8:6:86). The sialic acid elution was monitored using the fluorescence detector Shimadzu RF-10 AX L (Shimadzu, USA) at 448 nm emission and 373 nm excitation. Neu5Ac (Sigma-Aldrich, Germany) was used as reference standard for the retention time calculation and the quantification of the amount. Data were then normalized to wildtype (=100%).

4.4. Glycosphingolipid analysis of brain tissue

Mouse brains were collected from PBS-perfused female mice, shock-frozen on dry ice, and stored at −80 °C until usage. Frozen tissue was homogenized in chloroform/methanol (1:2 (v/v)) using the Precellys 24 tissue homogenizer with Precellys lysing kit (Bertin Instruments, Montigny-le-Bretonneux, France) 3 times for 5 seconds at 6500 rpm. Glycolipid extraction and xCGE-LIF analysis was performed as describe previously by Rossdam et al. (Rossdam et al., 2019). Briefly, brain homogenates were treated by sonication, cell debris and proteins were removed by centrifugation and the extract was transferred into a new vial. The extraction was repeated with chloroform/methanol (1:1 (v/v)) and chloroform/methanol (2:1 (v/v)), respectively and the pooled extracts were further purified on a Chromabond C_{18} ec polypropylene column (Macherey-Nagel, Düren, Germany). The extracted glycolipids were digested with LudgerZyme ceramide glycanase (CGase) from *H. medicinalis* (Ludger, Abingdon, UK). Released glycans were fluorescently labeled with 8-aminopyrene-1,3,6-trisulfonic acid (APTS; Sigma-Aldrich, Germany) and were subsequently analyzed by multiplexed capillary gel electrophoresis coupled to laser-induced fluorescence detection (xCGE-LIF). The analysis was carried out using an ABI PRISM 3100-*Avant* Genetic Analyzer (Thermo Fisher Scientific, Foster City, California, USA). Data were further processed using the GeneMapper Software (v.3.7.; Applied Biosystem, USA).

4.5. RNA isolation of brain samples, cDNA synthesis by reverse transcription of RNA and semi-quantitative real-time polymerase chain reaction (sqRT-PCR)

Half brains were collected after PBS perfusion of mice and immediately homogenized in QIAzol Lysis reagent (Qiagen, Germany) and stored at −80 °C until usage. Total RNA was extracted according to the manufacturer's manual using the RNeasy Mini kit (Qiagen #74106, Hilden, Germany). Reverse transcription of RNA was performed using the SuperScript III reverse transcriptase and hexamer random primers (both Invitrogen, Germany) according to the Invitrogen protocol for SuperScript First-Strand Synthesis. Semi-quantitative real-time polymerase chain reaction (sqRT-PCR) with specific oligonucleotides (Suppl. Table 1) was performed according to the manufacturer's protocol using the SYBR Green PCR Master Mix (Invitrogen, Germany) and the Mastercycler epigradient S (Eppendorf, Wesseling-Berzdorf, Germany). Gene transcripts of the housekeeping gene *glyceraldehyde-3-phosphate dehydrogenase (Gapdh)* were applied as internal RNA loading control. Amplification specificity was confirmed by analysis of the melting curves. Results were analyzed with the Mastercycler ep realplex software (Eppendorf, Germany) after establishing the reaction efficiency for each primer pair. Values were normalized with their respective *Gapdh* values and quantified using the delta delta-CT method.

4.6. RNA sequencing, bioinformatic data processing and analysis

Total RNA was extracted from brains of 4 female GNE+/− mice and 4 wildtype littermates as described above plus an additional −20 °C overnight incubation to ensure small RNA precipitation. Quality controls and differences in *Gne* transcription were pre-validated by sqRT-PCR. Quality and concentration of the RNA was determined using the Agilent 2100 Bioanalyzer and RNA 6000 Nano kits (Agilent Technologies, Santa Clara, California, USA). Only good-quality RNA (no contamination or degradation, RIN >9) was used. The sequencing of the samples was done at the Genomics Core Facility in EMBL Heidelberg, Germany. Briefly, for sequencing of the brain total RNA samples, single-end and unstranded reads were used and the samples were processed in an Illumina CBot. Libraries were sequenced on a NextSeq 500 machine (Illumina, San Diego, California, USA) following the manufacturer's instructions. The quality of raw reads was checked by FastQC version 0.11.3 (https://www.bioinformatics.babraham.ac.uk/projects/fastqc/). Cutadapt6 version 1.8.1 was used to trim low quality reads (−q 30 parameter), remove Illumina adapters (-a parameter) and to remove reads shorter than 20 bases (−m 20 parameter) with an error tolerance of 10% (−e 0.1 parameter). Additionally, reads mapping to ribosomal RNA species were removed using SortMeRNA7 with the parameters "--other; --log; -a; -v; --fastx enabled".

The RNA reads were processed by FastQC version 0.11.3 to test for bias. As no obvious bias was observed, the reads were mapped to the mouse genome mm10 by using the gene annotation downloaded from Ensembl (GRCm38.p3, release 79) and by using the Spliced Transcripts Alignment to a Reference (STAR) version 2.5.2b and the optimized parameters (Baruzzo et al., 2017). Briefly, the tweaked command arguments were:

```
--twopassMode Basic --outSAMunmapped Within
--limitOutSJcollapsed 1,000,000 \
--limitSjdbInsertNsj 1,000,000 --outFilterMultimapNmax 100
--outFilterMismatchNmax 33 \
```

--outFilterMismatchNoverLmax 0.3 --seedSearchStartLmax 12 --alignSJoverhangMin 15 \
--alignEndsType Local --outFilterMatchNminOverLread 0 --outFilterScoreMinOverLread 0.3 --winAnchorMultimapNmax 50 --alignSJDBoverhangMin 3

The reads were further counted using the function featureCounts from the R package Rsubreads (v1.26; Liao et al., 2013) and the statistical analysis was performed using the R package DESeq2 (v1.15; Love et al., 2014). Most computation and plotting were done using R (v3.4.0; R Core Team, 2017) and RStudio (v1.1; RStudio Team, 2016). Principle component analysis was computed using the function plotPCA() from the DESeq2 package and plotted by the R package factoextra (v1.0.4; Kassambara and Mundt, 2017). Of note, the logFoldChange were shrunk using the apeglm R package that preserves genuine difference in gene expression (v1.2.1; Zhu et al., 2018). Other plots were done using the R package ggplot2 (v2.1; Wickham, 2009) and the collection of packages tidyverse (v1.1; Wickham et al., 2019). For Ingenuity Pathway Analysis (IPA; Qiagen), the list of differentially expressed genes in GNE+/− mice (false discovery rate: <0.1) was uploaded in the IPA tool (Ingenuity Systems, www.ingenuity.com). The significance of the association of the genes with a function or canonical pathway was measured by Fisher's exact test. For Upstream Regulator Analysis only regulatory proteins were considered.

4.7. Immunohistochemistry of brain tissue

Left brain hemisphere of mice was immersion-fixed in 4% PFA overnight at 4 °C, cryoprotected in 30% sucrose (Roth, Karlsruhe, Germany), and then embedded and frozen in O.C.T. Compound, Tissue Tek (Sakura/Fisher Scientific, Schwerte, Germany). Embedded brains were cut into 20 μm sagittal sections using a cryostat Microm Cryo Star HM 560 (Thermo Scientific, Schwerte, Germany).

For surface sialylation analysis, sections (lateral: 1.30−1.40 mm) were incubated in blocking solution (10% BSA + 0.1% Triton X-100 + 5% NGS) for 25 minutes at room temperature. Primary antibody against PSA-NCAM (clone: 2-2B; 1:200; Millipore MAB5324, Germany) and A2B5 (clone: 105; 1:200; Invitrogen #433110, Germany), diluted in blocking solution, was added and sections were incubated overnight at 4 °C. After careful washing steps (3 × 5 minutes) with PBS, sections were incubated with Cy3-conjugated goat anti-mouse IgG F(ab')2 (1:250; Dianova #115-166-072, Hamburg, Germany) in blocking solution for 2 hours, carefully washed again with PBS before incubating with 4′,6-diamidino-2-phenylindole (DAPI; 1:10,000; Sigma-Aldrich, Germany). Sections were mounted with Aqua-Polymount (Polysciences Inc., Hirschberg a. d. Bergstraße, Germany). Three images were taken above the dentate gyrus of the hippocampus at a magnification of 40× and a zoom of 2.5× using the confocal microscope FluoView 1000 (Olympus, Hamburg, Germany) and the FluoView software (v3.1, Olympus, Germany).

For neuronal cell density analysis, sections (lateral: 1.10−1.20 mm) were incubated in blocking solution (10% BSA + 0.2% Triton X-100 + 5% NGS) for one hour at room temperature. Primary antibodies for tyrosine hydroxylase (TH; 1:500; Sigma-Aldrich #T8700, Germany) and neuronal nuclei (NeuN; 1:500; Millipore #MAB377, Germany), diluted in blocking solution, were added and sections were incubated for 2 hours at room temperature. After washing the sections 3 times with saline, the according secondary antibodies (Alexa Fluor 488-conjugated goat-anti-rabbit; 1:500; Invitrogen #A11008 and Cy3-conjugated goat anti-mouse IgG F(ab') 2; 1:200; Dianova #115-166-072, both Germany), diluted in blocking solution, were added and incubated for another 2 hours at room temperature. The sections were washed again twice and stained with DAPI (1:10,000) before mounting with mowiol (Kremer Pigmente, Aichstetten, Germany). Images of either whole substantia nigra or of whole hippocampus area were taken with an apotome (AxioImager.Z1, Zeiss, Jena, Germany) using the MosaiX function. Single images were post-processed using the stitching and processing tool from the AxioVisio software (v4.8.2.0, Zeiss, Germany).

For synaptic density analysis, sagittal sections (lateral: 1.20 mm−1.30 mm) were incubated in blocking solution (2% BSA + 0.2% Triton X-100 in PBS) for one hour at room temperature. Primary antibodies for postsynaptic density protein 95 (PSD95, clone: 7E3-1B8; 1:200; Thermo Scientific #MA1046, Germany) and for vesicular glutamate transporter 1 (vGlut1; 1:500; Synaptic Systems GmbH #135303, Göttingen, Germany) in diluent solution (0.5% BSA + 0.05% Triton X-100 in PBS) were added and incubated for 3 days at 4 °C. After washing the sections 3 times with saline the according secondary antibodies (Alexa Fluor 488-conjugated goat-anti-mouse; 1:500; Invitrogen #A11001 and Cy3-conjugated goat anti-rabbit IgG F(ab')2; 1:200; Dianova #111-165-047, both Germany) in diluent solution were added and incubated overnight at 4 °C. The sections were washed again twice and immunohistologically stained with DAPI (1:10,000) before mounting with Aqua-Polymount (Polysciences Inc., Germany). Three images were taken above the dentate gyrus of the hippocampus at 0.33 μm intervals over 15 optical sections with an SP8 confocal microscope and the LAS-X software (both Leica, Wetzlar, Germany).

For the quantification of microglia, sagittal sections (lateral: 1.20 mm−1.30 mm) were incubated in blocking solution (10% BSA + 0.25% Triton X-100 in PBS) for 2 hours at room temperature, followed by incubation in primary antibodies directed against Iba1 (1:500; IBA1/AIF1, Synaptic Systems GmbH #234003, Germany) in incubation solution (5% BSA + 0.05% Triton X-100 in PBS) overnight at 4 °C. After thorough washing with saline, sections were stained with the corresponding secondary antibody (Alexa Fluor 488-conjugated goat-anti-rabbit IgG; 1:400; Invitrogen #A11008) in incubation solution for 2 hours at room temperature. After washing with saline, sections were stained for nuclei (DAPI, 1:10,000) for 30 seconds and then covered with Aqua-Polymount (Polysciences Inc., Germany). Three z-stacks of 20 × 1 μm were taken above the dentate gyrus of the hippocampus for each mouse with an SP8 confocal microscope and the LAS-X software (both Leica, Germany).

All images were number-coded and analyzed by a blinded investigator using the software ImageJ (version v1.50i; NIH, MBF, USA). Positions of the recordings were defined according to the mouse brain atlas of Paxinos & Franklin.

4.8. Surface sialylation analysis

For overall sialic acid expression, total fluorescence integrated density of PSA-NCAM or A2B5 was measured in each image using ImageJ (v1.50i; MIH, MBF, USA). Mean background fluorescence was measured based on a secondary antibody control and subtracted in the complete area measured per image to calculate real mean fluorescence intensity per area per mouse.

4.9. Neuronal and synaptic density analysis

TH- and NeuN-positive cells within the substantia nigra pars compacta (SN pc) or only NeuN-positive cells in the CA3 area of the hippocampus were counted and the area was measured. Double-labeling with DAPI-positive cells was used as control. The neuronal density was calculated as number of counted cells per area and normalized to 3 month old wildtype mice. At least 3 images per mouse were analyzed. For synaptic density, maximum projection of the z-stack images was processed using ImageJ

(v1.50i). The maximum projection of the vGlut1- and PSD95-positive z-stack images was then further analyzed using the ImageJ plug-in Puncta Analyzer as described elsewhere (Ippolito and Eroglu, 2010).

4.10. Morphological analysis of microglia

Maximum projections of the Iba1-/DAPI-double positive z-stack images were generated and analyzed in ImageJ (v.1.52u) using custom-written plugins. Microglia density was quantified by counting Iba1-/DAPI-double-positive cell per area in each image and calculating the average for each mouse. To determine the overall Iba1 expression, total fluorescence integrated density was measured and analyzed as described for surface sialylation (see above). For microglia arborization, in each image, up to 3 microglial cells were randomly selected by a trained and blinded investigator and analyzed similar to what has been described (Plescher et al., 2018). For each microglial cell, a polygonal region of interest (ROI) that circumscribed all microglial processes belonging to that cell was set. From each ROI a single cell image was generated. Each single cell image was subjected to a custom-written image segmentation plugin: 1.) An intensity-threshold (MinError-algorithm, implemented in ImageJ) was calculated in a 0.5-fold scaled copy of the original image, of which the single cell image had been derived, based on the pixel intensities inside the convex hull of the ROI that was used to produce the single-cell image; 2.) The threshold was applied to the single-cell image by setting all pixel intensities below the threshold to 0.0. Segmented images were subjected to a custom-written particle filter that removed all particles below 15 px (corresponding to about 0.44 μm^2) from the image. The area (referred to as "area covered") was calculated. To determine the "total tree length", the "number of branches", the "number of junctions", and the "number of tips", the particle-filtered single cell image was Gauss-filtered (sigma 1.0), skeletonized using the Fiji plugin "Skeletonize3D" (Arganda-Carreras et al., 2010), and analyzed using the Fiji plugin "Analyze Skeleton" (Arganda-Carreras et al., 2010).

To quantify the soma area, maximum projections used for morphology characterization were processed in ImageJ as follows: 1.) *Subtract Background* (radius: 100 px, corresponding to about 17.2 μm); 2.) Gaussian Blur (sigma = 2); 3.) Make a binary image by applying an intensity threshold determined by the ImageJ threshold algorithm Otsu; 4.) Minimum Filter (5 px, corresponding to 0.68 μm); 5.) Maximum Filter (5 px, corresponding to 0.68 μm). This procedure allowed to remove fine structures from the image while keeping thicker structures like the soma. Finally, the area of each remaining soma structure was determined.

4.11. Statistical analysis

Data are presented as mean ± SEM or mean + SEM (if not stated otherwise) of at least 3 mice. N-numbers represent the number of investigated mice. Per mouse at least 3 independent data points were collected and analyzed. Data with one variable were tested for normality and then analyzed by Student's t-test or if group number >2 by one-way ANOVA followed by Bonferroni *post hoc* test or Dunnett's T3 method comparing all columns using the IBM SPSS Statistics (v.22; IBM Corporation, Germany). For more than one variable, a linear model (multiple linear regression) including an interaction term was applied, followed by a pairwise comparison with LSD-post hoc correction using the computer software STATA/IC (v13.1; Stata Corp, USA). The Breusch-Pagan/Cook-Weisberg test for heteroscedasticity was performed to assess the equality of variances in the linear model. If variances were significantly different a robust linear model including an interaction term was chosen for further analysis. For easier reading only significant pairwise comparisons were indicated in the figures when a linear model was applied. Data are considered as significant if $^{*}p \leq 0.050$, $^{**}p \leq 0.010$, or $^{***}p \leq 0.001$.

Disclosure statement

The authors have no conflicting financial interests.

Acknowledgements

We thank Rita Jietou and Sharon Weingarten for excellent technical support. This project was funded by the Deutsche Forschungsgemeinschaft (DFG; German Research Foundation) via LI2833/1-1 (No. 317148800) and via FOR2953 (for H.N. NE507/16-1 Nr. 432190414 and for F.F.R.B. BU2920/4-1 Nr. 432218849). C.K. and H.N. received funding from the Innovative Medicines Initiative 2 Joint Undertaking under grant agreement No 115976 (PHAGO). J.N.H. is holding a PhD fellowship by the Boehringer Ingelheim Fonds. We would like to acknowledge the assistance of the Microscopy Core Facility of the Medical Faculty at the University of Bonn and we would like to thank EMBL Gene Core at Heidelberg for support with high-throughput sequencing. The experiments presented in this paper were carried out using the HPC facilities of the University of Luxembourg (Varrette et al., 2014).

Author contributions: C.K., B.LG., and H.N. conceived and designed the project with input from L.S.; C.K. conducted all animal experiments, tissue sampling, the laboratory experiments, including flow cytometry, immunohistological stainings of brain tissue, RNA isolation, cDNA synthesis and sqRT-PCR and data analysis with inputs from B.LG. and H.N.; J.N.H. analyzed the morphological microglia reconstruction with inputs from C.K.; A.G., D.G., and L.S. conducted the RNA sequencing, bioinformatics data processing and analysis with input of T.S. and C.K.; V.S.G. conducted the HPLC-based sialic acid determination in tissue with input from R.H.; C.R. conducted the glycosphingolipid analysis of brain tissue with input from F.F.R.B.; C.K., B.LG., and H.N. wrote the manuscript. All authors contributed to manuscript writing and reviewed the manuscript.

Data availability: The sequencing data is deposited in the European Nucleotide Archive (E-MTAB-7790). All other data are available from the authors upon reasonable request.

Appendix A. Supplementary data

Supplementary data to this article can be found online at https://doi.org/10.1016/j.neurobiolaging.2020.01.008.

References

Abeln, M., Albers, I., Peters-Bernard, U., Flächsig-Schulz, K., Kats, E., Kispert, A., Tomlinson, S., Gerardy-Schahn, R., Münster-Kühnel, A., Weinhold, B., 2018. Sialic acid is a critical fetal defense against maternal complement attack. J. Clin. Invest. 129, 422–436.

Arganda-Carreras, I., Fernández-González, R., Muñoz-Barrutia, A., Ortiz-De-Solorzano, C., 2010. 3D reconstruction of histological sections: application to mammary gland tissue. Microsc. Res. Tech. 73, 1019–1029.

Baruzzo, G., Hayer, K.E., Kim, E.J., Di Camillo, B., FitzGerald, G.A., Grant, G.R., 2017. Simulation-based comprehensive benchmarking of RNA-seq aligners. Nat. Methods 14, 135–139.

Blatteis, C.M., Sehic, E., 1998. Cytokines and fever. Ann. N. Y. Acad. Sci. 840, 608–618.

Blaum, B.S., Hannan, J.P., Herbert, A.P., Kavanagh, D., Uhrín, D., Stehle, T., 2015. Structural basis for sialic acid-mediated self-recognition by complement factor H. Nat. Chem. Biol. 11, 77–82.

Bodea, L.-G.L.-G., Wang, Y., Linnartz-Gerlach, B., Kopatz, J., Sinkkonen, L., Musgrove, R., Kaoma, T., Muller, A., Vallar, L., Di Monte, D.A., Balling, R., Neumann, H., 2014. Neurodegeneration by activation of the microglial complement-phagosome pathway. J. Neurosci. 34, 8546–8556.

Boukhris, A., Schule, R., Loureiro, J.L., Lourenço, C.M., Mundwiller, E., Gonzalez, M.A., Charles, P., Gauthier, J., Rekik, I., Acosta Lebrigio, R.F., Gaussen, M., Speziani, F., Ferbert, A., Feki, I., Caballero-Oteyza, A., Dionne-Laporte, A., Amri, M., Noreau, A., Forlani, S., Cruz, V.T., Mochel, F., Coutinho, P., Dion, P., Mhiri, C., Schols, L., Pouget, J., Darios, F., Rouleau, G.A., Marques, W., Brice, A., Durr, A., Zuchner, S., Stevanin, G., 2013. Alteration of ganglioside biosynthesis responsible for complex hereditary spastic paraplegia. Am. J. Hum. Genet. 93, 118–123.
Cherubini, E., Miles, R., 2015. The CA3 region of the hippocampus: how is it? What is it for? How does it do it? Front. Cell. Neurosci. 9, 19.
Cohen, M., Varki, A., 2010. The sialome—far more than the sum of its parts. OMICS 14, 455–464.
Cremer, H., Lange, R., Christoph, A., Plomann, M., Vopper, G., Roes, J., Brown, R., Baldwin, S., Kraemer, P., Scheff, S., Barthels, D., Rajewsky, K., Wille, W., 1994. Inactivation of the N-CAM gene in mice results in size reduction of the olfactory bulb and deficits in spatial learning. Nature 367, 455–459.
Crocker, P.R., Paulson, J.C., Varki, A., 2007. Siglecs and their roles in the immune system. Nat. Rev. Immunol. 7, 255–266.
De Castro E Silva, E., Luz, P.A., Magrani, J., Andrade, L., Miranda, N., Pereira, V., Fregoneze, J.B., 2006. Role of the central opioid system in the inhibition of water and salt intake induced by central administration of IL-1beta in rats. Pharmacol. Biochem. Behav. 83, 285–295.
Di Giovanni, G., Pessia, M., Di Maio, R., 2012. Redox sensitivity of tyrosine hydroxylase activity and expression in dopaminergic dysfunction. CNS Neurol. Disord. Drug Targets 11, 419–429.
Eckhardt, M., Bukalo, O., Chazal, G., Wang, L., Goridis, C., Schachner, M., Gerardy-Schahn, R., Cremer, H., Dityatev, A., 2000. Mice deficient in the polysialyltransferase ST8SiaIV/PST-1 allow discrimination of the roles of neural cell adhesion molecule protein and polysialic acid in neural development and synaptic plasticity. J. Neurosci. 20, 5234–5244.
Filipello, F., Morini, R., Corradini, I., Zerbi, V., Canzi, A., Michalski, B., Erreni, M., Markicevic, M., Starvaggi-Cucuzza, C., Otero, K., Piccio, L., Cignarella, F., Perrucci, F., Tamborini, M., Genua, M., Rajendran, L., Menna, E., Vetrano, S., Fahnestock, M., Paolicelli, R.C., Matteoli, M., 2018. The microglial innate immune receptor TREM2 is required for synapse elimination and normal brain connectivity. Immunity 48, 979–991.e8.
Folch, J., Lees, M., Sloane Stanley, G.H., 1957. A simple method for the isolation and purification of total lipides from animal tissues. J. Biol. Chem. 226, 497–509.
Gagiannis, D., Orthmann, A., Danßmann, I., Schwarzkopf, M., Weidemann, W., Horstkorte, R., 2007. Reduced sialylation status in UDP-N-acetylglucosamine-2-epimerase/N- acetylmannosamine kinase (GNE)-deficient mice. Glycoconj. J. 24, 125–130.
Hall, B.S., Moda, R.N., Liston, C., 2015. Neurobiology of Stress Glucocorticoid mechanisms of functional connectivity changes in stress-related neuropsychiatric disorders. Neurobiol. Stress 1, 174–183.
Hanashima, S., Sato, C., Tanaka, H., Takahashi, T., Kitajima, K., Yamaguchi, Y., 2013. NMR study into the mechanism of recognition of the degree of polymerization by oligo/polysialic acid antibodies. Bioorg. Med. Chem. 21, 6069–6076.
Huang, Y.-X., Tuo, W.-W., Wang, D., Kang, L.-L., Chen, X.-Y., Luo, M., 2016. Restoring the youth of aged red blood cells and extending their lifespan in circulation by remodelling membrane sialic acid. J. Cell Mol Med 20, 294–301.
Ingiosi, A.M., Raymond, R.M., Pavlova, M.N., Opp, M.R., 2015. Selective contributions of neuronal and astroglial interleukin-1 receptor 1 to the regulation of sleep. Brain Behav. Immun. 48, 244–257.
Ippolito, D.M., Eroglu, C., 2010. Quantifying synapses: an immunocytochemistry-based assay to quantify synapse number. J. Vis. Exp. e2270.
Kassambara, A., Mundt, F., 2017. Factoextra: Extract and Visualize the Results of Multivariate Data Analyses. Available at: https://CRAN.R-project.org/package=factoextra. (Accessed 19 March 2019).
Keppler, O.T., 1999. UDP-GlcNAc 2-epimerase: a regulator of cell surface sialylation. Science 284, 1372–1376.
Kraft, A.D., McPherson, C.A., Harry, G.J., 2016. Association between microglia, inflammatory factors, and complement with loss of hippocampal mossy fiber synapses induced by trimethyltin. Neurotox. Res. 30, 53–66.
Kumar, D., Rizvi, S., 2013. Erythrocyte membrane bound and plasma sialic acid during aging. Biologia (Bratisl) 68, 762–765.
Liao, Y., Smyth, G.K., Shi, W., 2013. The Subread aligner: fast, accurate and scalable read mapping by seed-and-vote. Nucleic Acids Res. 41, e108.
Linnartz-Gerlach, B., Mathews, M., Neumann, H., 2014. Sensing the neuronal glycocalyx by glial sialic acid binding immunoglobulin-like lectins. Neuroscience 275, 113–124.
Linnartz-Gerlach, B., Schuy, C., Shahraz, A., Tenner, A.J., Neumann, H., 2016. Sialylation of neurites inhibits complement-mediated macrophage removal in a human macrophage-neuron co-culture system. Glia 64, 35–47.
Linnartz, B., Kopatz, J., Tenner, A.J., Neumann, H., 2012. Sialic acid on the neuronal glycocalyx prevents complement C1 binding and complement receptor-3-mediated removal by microglia. J. Neurosci. 32, 946–952.
Liston, C., Cichon, J.M., Jeanneteau, F., Jia, Z., Chao, M.V., Gan, W., 2013. Circadian glucocorticoid oscillations promote learning- dependent synapse formation and maintenance. Nat. Neurosci. 16, 698–705.
Love, M.I., Huber, W., Anders, S., 2014. Moderated estimation of fold change and dispersion for RNA-seq data with DESeq2. Genome Biol. 15, 550.
Lutz, H.U., Bogdanova, A., 2013. Mechanisms tagging senescent red blood cells for clearance in healthy humans. Front. Physiol. 4, 387.
Luz, P.A., Andrade, L., Miranda, N., Pereira, V., Fregoneze, J., De Castro e Silva, E., 2006. Inhibition of water intake by the central administration of IL-1β in rats: role of the central opioid system. Neuropeptides 40, 85–94.
Luz, P.A., Saraiva, R., Almeida, T., Fregoneze, J.B., De Castro e Silva, E., 2009. Blockade of central kappa-opioid receptors inhibits the antidipsogenic effect of interleukin-1beta. Neuropeptides 43, 93–103.
Margolis, R.K., Margolis, R.U., 1983. Distribution and characteristics of polysialosyl oligosaccharides in nervous tissue glycoproteins. Biochem. Biophys. Res. Commun. 116, 889–894.
Mehdi, M.M., Singh, P., Rizvi, S.I., 2012. Erythrocyte sialic acid content during aging in humans: correlation with markers of oxidative stress. Dis. Markers 32, 179–186.
Morimoto, A., Ono, T., Watanabe, T., Murakami, N., 1986. Activation of brain regions of rats during fever. Brain Res. 381, 100–105.
Murray, H.C., Low, V.F., Swanson, M.E.V., Dieriks, B.V., Turner, C., Faull, R.L.M., Curtis, M.A., 2016. Distribution of PSA-NCAM in normal, Alzheimer's and Parkinson's disease human brain. Neuroscience 330, 359–375.
Netea, M.G., Kullberg, B.J., Van der Meer, J.W., 2000. Circulating cytokines as mediators of fever. Clin. Infect. Dis. 31 (Suppl 5), S178–S184.
Norton, W.T., Poduslo, S.E., 1973. Myelination in rat brain: changes in myelin composition during brain maturation. J. Neurochem. 21, 759–773.
O'Ferrall, E.K., Sinnreich, M., 1993. GNE-related myopathy, GeneReviews®. University of Washington, Seattle (WA).
Ohmi, Y., Ohkawa, Y., Tajima, O., Sugiura, Y., Furukawa, K., Furukawa, K., 2014. Ganglioside deficiency causes inflammation and neurodegeneration via the activation of complement system in the spinal cord. J. Neuroinflammation 11, 61.
Ohmi, Y., Tajima, O., Ohkawa, Y., Yamauchi, Y., Sugiura, Y., Furukawa, K., Furukawa, K., 2011. Gangliosides are essential in the protection of inflammation and neurodegeneration via maintenance of lipid rafts: elucidation by a series of ganglioside-deficient mutant mice. J. Neurochem. 116, 926–935.
Paolicelli, R.C., Bolasco, G., Pagani, F., Maggi, L., Scianni, M., Panzanelli, P., Giustetto, M., Ferreira, T.A., Guiducci, E., Dumas, L., Ragozzino, D., Gross, C.T., 2011. Synaptic pruning by microglia is necessary for normal brain development. Science 333, 1456–1458.
Plescher, M., Seifert, G., Hansen, J.N., Bedner, P., Steinhäuser, C., Halle, A., 2018. Plaque-dependent morphological and electrophysiological heterogeneity of microglia in an Alzheimer's disease mouse model. Glia 66, 1464–1480.
Pluvinage, J.V., Haney, M.S., Smith, B.A.H., Sun, J., Iram, T., Bonanno, L., Li, L., Lee, D.P., Morgens, D.W., Yang, A.C., Shuken, S.R., Gate, D., Scott, M., Khatri, P., Luo, J., Bertozzi, C.R., Bassik, M.C., Wyss-Coray, T., 2019. CD22 blockade restores homeostatic microglial phagocytosis in ageing brains. Nature 568, 187–192.
Pogoryelova, O., González Coraspe, J.A., Nikolenko, N., Lochmüller, H., Roos, A., 2018. GNE myopathy: from clinics and genetics to pathology and research strategies. Orphanet J. Rare Dis. 13, 70.
Qadri, S.M., Donkor, D.A., Nazy, I., Branch, D.R., Sheffield, W.P., 2018. Bacterial neuraminidase-mediated erythrocyte desialylation provokes cell surface aminophospholipid exposure. Eur. J. Haematol. 100, 502–510.
Qu, R., Sang, Q., Wang, X., Xu, Y., Chen, B., Mu, J., Zhang, Z., Jin, L., He, L., Wang, L., 2019. A homozygous mutation in CMAS causes autosomal recessive intellectual disability in a Kazakh family. Ann. Hum. Genet. 84, 46–53.
R Core Team, 2017. R: A Language and Environment for Statistical Computing. The R Foundation for Statistical Computing, Vienna, Austria. https://www.R-project.org/. (Accessed 19 March 2019).
Rachmilewitz, J., 2010. Glycosylation: an intrinsic sign of "Danger. Self Nonself 1, 250–254.
Rossdam, C., Konze, S.A., Oberbeck, A., Rapp, E., Gerardy-Schahn, R., von Itzstein, M., Buettner, F.F.R., 2019. Approach for profiling of glycosphingolipid glycosylation by multiplexed capillary gel electrophoresis coupled to laser-induced fluorescence detection to identify cell-surface markers of human pluripotent stem cells and derived cardiomyocytes. Anal Chem. 91, 6413–6418.
RStudio Team, 2016. RStudio. Integrated Development for R.
Saito, M., Kitamura, H., Sugiyama, K., 2001. The specificity of monoclonal antibody A2B5 to c-series gangliosides. J. Neurochem. 78, 64–74.
Sato, C., Kitajima, K., 2013. Disialic, oligosialic and polysialic acids: distribution, functions and related disease. J. Biochem. 154, 115–136.
Schafer, D.P., Lehrman, E.K., Kautzman, A.G., Koyama, R., Mardinly, A.R., Yamasaki, R., Ransohoff, R.M., Greenberg, M.E., Barres, B.A., Stevens, B., 2012. Microglia sculpt postnatal neural circuits in an activity and complement-dependent manner. Neuron 74, 691–705.
Schafer, D.P., Stevens, B., 2010. Synapse elimination during development and disease: immune molecules take centre stage. Biochem. Soc. Trans. 38, 476–481.
Schauer, R., 2009. Sialic acids as regulators of molecular and cellular interactions. Curr. Opin. Struct. Biol. 19, 507–514.
Schnaar, R.L., Gerardy-Schahn, R., Hildebrandt, H., 2014. Sialic acids in the brain: gangliosides and polysialic acid in nervous system development, stability, disease, and regeneration. Physiol. Rev. 94, 461–518.
Schwarzkopf, M., Knobeloch, K.-P., Rohde, E., Hinderlich, S., Wiechens, N., Lucka, L., Horak, I., Reutter, W., Horstkorte, R., 2002. Sialylation is essential for early development in mice. Proc. Natl. Acad. Sci. U. S. A. 99, 5267–5270.
Simpson, M.A., Cross, H., Proukakis, C., Priestman, D.A., Neville, D.C.A., Reinkensmeier, G., Wang, H., Wiznitzer, M., Gurtz, K., Verganelaki, A., Pryde, A., Patton, M.A., Dwek, R.A., Butters, T.D., Platt, F.M., Crosby, A.H., 2004. Infantile-onset symptomatic epilepsy syndrome caused by a homozygous loss-of-function mutation of GM3 synthase. Nat. Genet. 36, 1225–1229.
Sousa, N., Lukoyanov, N.V., Madeira, M.D., Almeida, O.F., Paula-Barbosa, M.M., 2000. Reorganization of the morphology of hippocampal neurites and synapses after

stress-induced damage correlates with behavioral improvement. Neuroscience 97, 253–266.
Stevens, B., Allen, N.J., Vazquez, L.E., Howell, G.R., Christopherson, K.S., Nouri, N., Micheva, K.D., Mehalow, A.K., Huberman, A.D., Stafford, B., Sher, A., Litke, A.M., Lambris, J.D., Smith, S.J., John, S.W.M.M., Barres, B.A., 2007. The classical complement cascade mediates CNS synapse elimination. Cell 131, 1164–1178.
Svennerholm, L., 1994. Designation and Schematic Structure of Gangliosides and Allied Glycosphingolipids. Prog. Brain Res. 101, XI–XIV.
Svennerholm, L., Boström, K., Fredman, P., Månsson, J.E., Rosengren, B., Rynmark, B.M., 1989. Human brain gangliosides: developmental changes from early fetal stage to advanced age. Biochim. Biophys. Acta 1005, 109–117.
Svennerholm, L., Boström, K., Jungbjer, B., 1997. Changes in weight and compositions of major membrane components of human brain during the span of adult human life of Swedes. Acta Neuropathol. 94, 345–352.
Tettamanti, G., Bonali, F., Marchesini, S., Zambotti, V., 1973. A new procedure for the extraction, purification and fractionation of brain gangliosides. Biochim. Biophys. Acta 296, 160–170.
Varki, A., 2011. Since there are PAMPs and DAMPs, there must be SAMPs? Glycan "self-associated molecular patterns" dampen innate immunity, but pathogens can mimic them. Glycobiology 21, 1121–1124.
Varrette, S., Bouvry, P., Cartiaux, H., Georgatos, F., 2014. Management of an academic HPC cluster: the UL experience. In: 2014 International Conference on High Performance Computing & Simulation (HPCS). IEEE, Bologna, pp. 959–967.
Wang, Y., Neumann, H., 2010. Alleviation of neurotoxicity by microglial human Siglec-11. J. Neurosci. 30, 3482–3488.
Wei, M., Wang, P.G., 2019. Desialylation in physiological and pathological processes: new target for diagnostic and therapeutic development. Prog. Mol. Biol. Transl. Sci. 162, 25–57.
Wickham, H., Averick, M., Bryan, J., Chang, W., McGowan, L., François, R., Grolemund, G., Hayes, A., Henry, L., Hester, J., Kuhn, M., Pedersen, T., Miller, E., Bache, S., Müller, K., Ooms, J., Robinson, D., Seidel, D., Spinu, V., Takahashi, K., Vaughan, D., Wilke, C., Woo, K., Yutani, H., 2019. Welcome to the tidyverse. J Open Source Softw 4, 1686.
Wickham, H., 2009. ggplot2: Elegant Graphics for Data Analysis. Springer-Verlag, New York, NY.
Yamashita, T., Wu, Y.-P., Sandhoff, R., Werth, N., Mizukami, H., Ellis, J.M., Dupree, J.L., Geyer, R., Sandhoff, K., Proia, R.L., 2005. Interruption of ganglioside synthesis produces central nervous system degeneration and altered axon-glial interactions. Proc. Natl. Acad. Sci. U. S. A. 102, 2725–2730.
Yu, R.K., Macala, L.J., Taki, T., Weinfield, H.M., Yu, F.S., 1988. Developmental changes in ganglioside composition and synthesis in embryonic rat brain. J. Neurochem. 50, 1825–1829.
Zhu, A., Ibrahim, J.G., Love, M.I., 2018. Heavy-tailed prior distributions for sequence count data: removing the noise and preserving large differences. Bioinformatics 35, 2084–2092.